nature genetics

LETTERS

https://doi.org/10.1038/s41588-020-0681-7

Check for updates

Chromatin binding of FOXA1 is promoted by LSD1-mediated demethylation in prostate cancer

Shuai Gao[1,7], Sujun Chen[2,3,7], Dong Han[1], Zifeng Wang[1], Muqing Li[1], Wanting Han[1], Anna Besschetnova[1], Mingyu Liu[1], Feng Zhou[1,4], David Barrett[1], My Phu Luong[1], Jude Owiredu[1,5], Yi Liang[3], Musaddeque Ahmed[3], Jessica Petricca[2,3], Susan Patalano[1], Jill A. Macoska[1], Eva Corey[6], Sen Chen[5], Steven P. Balk[5]✉, Housheng Hansen He[2,3]✉ and Changmeng Cai[1]✉

FOXA1 functions as a pioneer transcription factor by facilitating the access to chromatin for steroid hormone receptors, such as androgen receptor and estrogen receptor[1–4], but mechanisms regulating its binding to chromatin remain elusive. LSD1 (KDM1A) acts as a transcriptional repressor by demethylating mono/dimethylated histone H3 lysine 4 (H3K4me1/2)[5,6], but also acts as a steroid hormone receptor coactivator through mechanisms that are unclear. Here we show, in prostate cancer cells, that LSD1 associates with FOXA1 and active enhancer markers, and that LSD1 inhibition globally disrupts FOXA1 chromatin binding. Mechanistically, we demonstrate that LSD1 positively regulates FOXA1 binding by demethylating lysine 270, adjacent to the wing2 region of the FOXA1 DNA-binding domain. Acting through FOXA1, LSD1 inhibition broadly disrupted androgen-receptor binding and its transcriptional output, and dramatically decreased prostate cancer growth alone and in synergy with androgen-receptor antagonist treatment in vivo. These mechanistic insights suggest new therapeutic strategies in steroid-driven cancers.

The androgen receptor (AR) coactivator function of LSD1 has been attributed to phosphorylation of histone H3 on threonine 6 (H3T6ph) and threonine 11, which may switch LSD1 substrate specificity from H3K4me1/2 to H3K9me1/2 (refs. [7–10]). However, we reported that the H3K4 demethylase activity of LSD1 persists at AR-regulated enhancers, including sites marked by H3T6ph[11], which argues against this model. As FOXA1 binds to AR-regulated enhancers marked with H3K4me1/2 before AR binding[12], and LSD1 chromatin binding substantially overlaps with FOXA1-binding sites[11], we hypothesized that LSD1 may regulate the accessibility of AR-mediated enhancers through interactions with FOXA1. Comprehensive ChIP–seq studies were carried out in LNCaP prostate cancer (PCa) cells grown in steroid-depleted medium to minimize the feedback effect of AR on FOXA1 chromatin binding[13]. As shown in Fig. 1a, LSD1-binding sites were associated with high levels of FOXA1 and active enhancer marks. Although we previously showed that FOXA1 binding is decreased by LSD1 silencing[11], it was unclear whether the catalytic activity of LSD1 is required (LSD1 can also function as a scaffold protein[14,15]). As shown in Fig. 1b–d and Extended Data Fig. 1a–d, LSD1-inhibitor treatments (GSK2879552, S2101 (refs. [16,17])) led to a rapid and dramatic decrease in global FOXA1 binding. This finding was subsequently validated in LNCaP and CWR22-RV1 PCa cells with LSD1 inhibition or silencing, and FOXA1 or AR protein expression was not affected by the treatments (Fig. 1e–g and Extended Data Fig. 1e–k). Moreover, overexpressing wild type (WT) LSD1, but not the demethylase-deficient K661A mutant, increased FOXA1 binding (Extended Data Fig. 1l,m).

Since FOXA1 de-compacts chromosome at enhancers, we next determined whether LSD1 inhibition suppresses chromatin opening at the binding sites. Using ATAC–seq, we showed that LSD1 inhibition markedly decreased the chromosome accessibility at FOXA1-occupied sites before androgen stimulation (Fig. 1h–i). LSD1 inhibition also led to rapid decreases in DNase hypersensitivity (DHS) and acetylated H3K27 (H3K27ac), confirming reduced opening of these regions before AR binding (Extended Data Fig. 2a–d). Importantly, the levels of H3K4me2 at LSD1-FOXA1 co-occupied sites were not strongly affected by LSD1 inhibition at 4 h, but eventually increased at 24 h (Fig. 1j), indicating that the disruption of FOXA1 binding by LSD1 inhibition (maximum reduction at 4 h) is mediated by a mechanism that is independent of H3K4 demethylation. Moreover, FOXA1 binding at AR-independent regulatory sites in PCa cells or estrogen receptor (ER)-mediated enhancer sites in breast cancer cells was also decreased by LSD1 inhibition (Extended Data Fig. 3a–c). Together, these data suggest that LSD1 globally maintains FOXA1 chromatin binding and regulates the opening of FOXA1-dependent enhancers via a specific molecular mechanism independent of its H3K4 demethylase acitivity.

Since AR chromatin binding is dependent on FOXA1, we next hypothesized that LSD1 inhibition may impair AR recruitment to enhancers. Notably, LSD1-inhibitor treatment in the presence of androgens markedly decreased the global AR chromatin binding, the levels of AR-induced DHS[18] and the recruitment of an AR coactivator, p300 (Fig. 2a–e and Extended Data Fig. 4a,b). Interestingly, this observation is in contrast to studies using approaches to silence FOXA1 expression, which indicate major reprogramming of AR cistrome[19,20]. A possible explanation is that LSD1 inhibition leads to decreased FOXA1 binding, which may still be sufficient to promote weaker recruitment of AR, while FOXA1 silencing forces AR to occupy alternative sites pioneered by other factors. Nonetheless, decreased AR binding by LSD1 inhibition broadly impaired the

[1]Center for Personalized Cancer Therapy, University of Massachusetts Boston, Boston, MA, USA. [2]Department of Medical Biophysics, University of Toronto, Toronto, Ontario, Canada. [3]Princess Margaret Cancer Center/University Health Network, Toronto, Ontario, Canada. [4]Department of Urology, The First Affiliated Hospital, School of Medicine, Zhejiang University, Hangzhou, China. [5]Hematology-Oncology Division, Department of Medicine, Beth Israel Deaconess Medical Center and Harvard Medical School, Boston, MA, USA. [6]Department of Urology, University of Washington, Seattle, WA, USA. [7]These authors contributed equally: Shuai Gao, Sujun Chen. ✉e-mail: sbalk@bidmc.harvard.edu; hansenhe@uhnresearch.ca; changmeng.cai@umb.edu

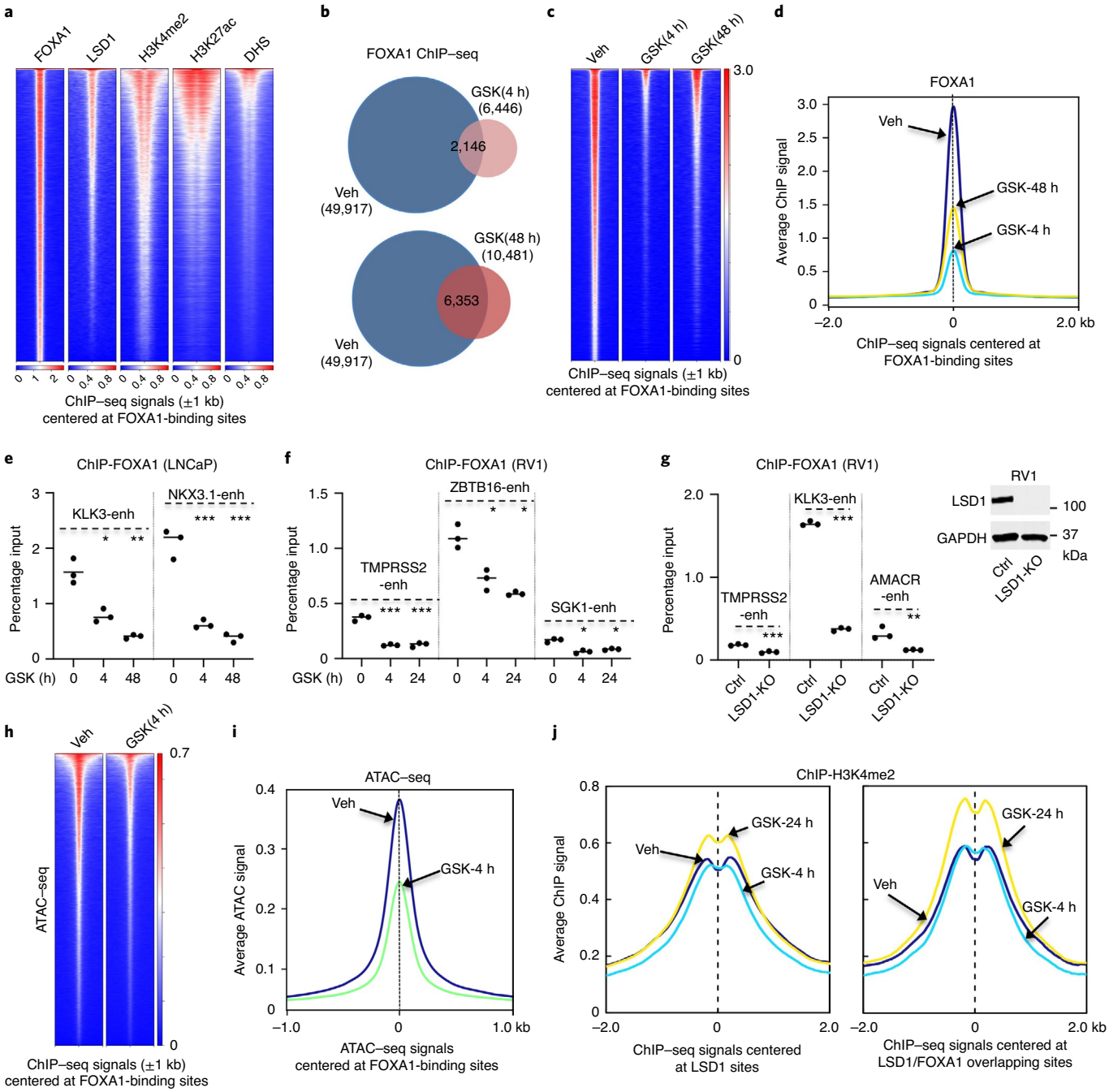

Fig. 1 | LSD1 inhibition disrupts global chromatin binding of FOXA1. a, The heat map view for FOXA1, LSD1, H3K4me2, H3K27ac and DHS ChIP–seq signal intensity at FOXA1-binding sites in LNCaP cells (FOXA1/AR positive, AR-V7 negative) grown in 5% CSS (hormone-depleted FBS). **b**–**d**, FOXA1 ChIP–seq (using antibody no. 1) was performed in LNCaP cells treated with 50 μM GSK2879552 at 4 h or 48 h. **b**, Overlap of FOXA1-binding sites between vehicle (Veh) and LSD1 inhibitors treated cells. **c**, The heat map view for FOXA1 ChIP–seq signal intensity. **d**, The mean of FOXA1 ChIP–seq signals at all FOXA1-binding sites (Veh versus GSK-4 h: $P = 2.5 \times 10^{-5}$; Veh versus GSK-48 h: $P = 0.056$). **e**,**f**, ChIP–qPCR for FOXA1 binding at *KLK3/NKX3.1* enhancer sites in LNCaP (**e**) or CWR22-RV1 (**f**) cells (FOXA1/AR positive, AR-V7 positive) treated with GSK2879552 for the indicated time. **g**, A LSD1-knockout (KO) cell line was established in CWR22-RV1 cells by using the CRISPR–Cas9 approach (by sgRNA targeting *LSD1*). LSD1 expression was immunoblotted in the LSD1-KO line versus the control (Ctrl) line. **h**, ATAC–seq was performed in LNCaP cells treated with vehicle or GSK2879552 at 4 h. The heat map view for ATAC–seq signal intensity at FOXA1-binding sites is shown. **i**, The mean of ATAC–seq signals at FOXA1-binding sites (Veh versus GSK-4 h: $P = 6.2 \times 10^{-20}$). **j**, The mean of H3K4me2 ChIP–seq signals at LSD1-binding sites (Veh versus GSK-4 h: $P = 0.86$; Veh versus GSK-48 h: $P = 6.1 \times 10^{-14}$) or LSD1/FOXA1 overlapping sites (Veh versus GSK-4 h: $P = 7.8 \times 10^{-5}$; Veh versus GSK-48 h: $P = 1.9 \times 10^{-22}$). Not significant (NS), $P > 0.05$; *$0.001 < P < 0.01$; **$0.01 < P < 0.05$; ***$P < 0.001$.

expression of direct AR-activated genes (Extended Data Fig. 4c–f). Moreover, overexpression of LSD1-WT, but not the K661A mutant, enhanced AR binding and increased androgen-induced gene expression (Extended Data Fig. 4g,h). The effects of LSD1 inhibition on AR activity and cell growth were dependent on the doses of inhibitors and the levels of androgens or LSD1 expression

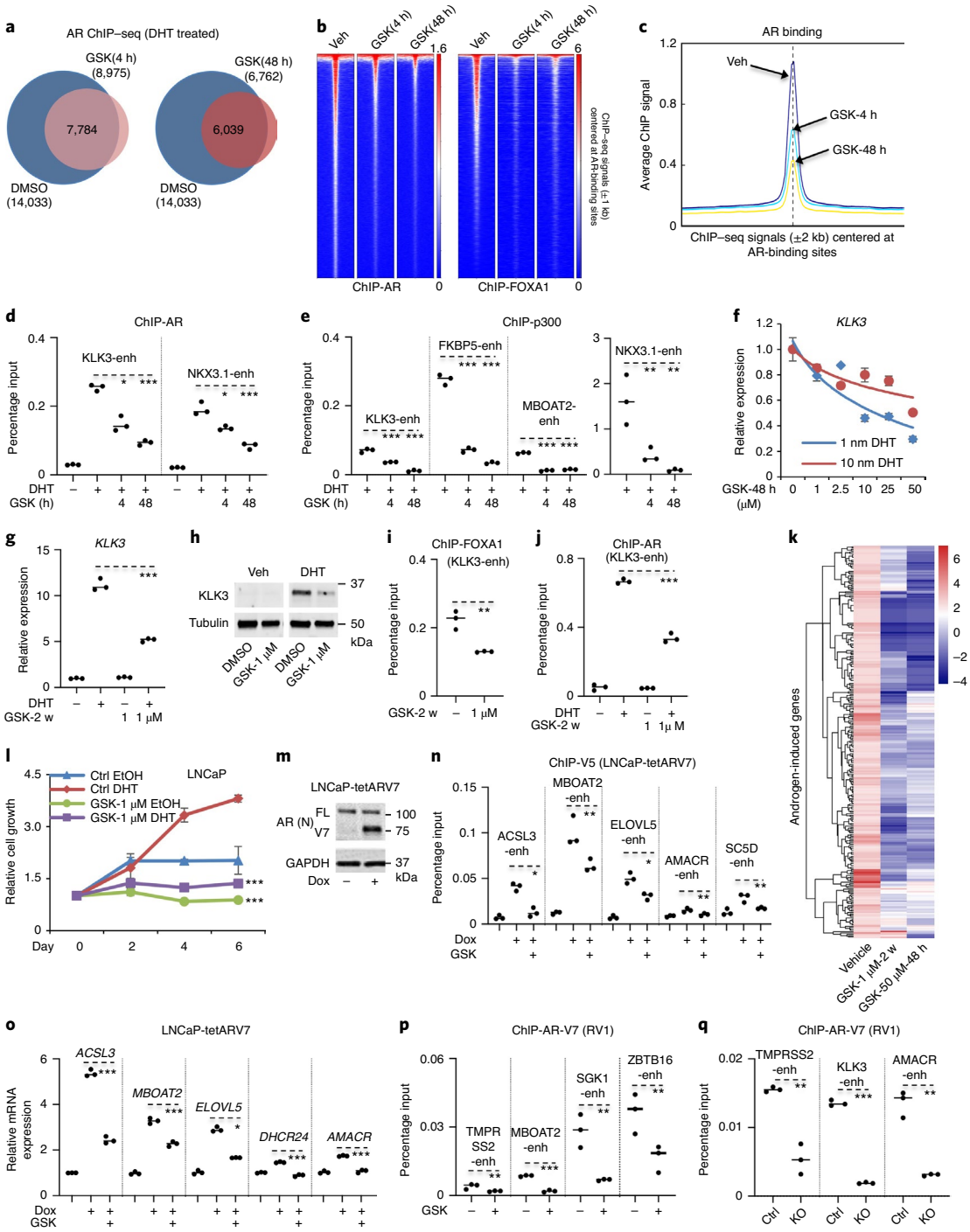

Fig. 2 | LSD1 inhibition broadly impairs AR recruitment and suppresses AR transcriptional activity. a–**c**, AR ChIP–seq analyses were performed in LNCaP cells treated with vehicle, DHT (10 nM for 4 h) or DHT (4 h) with pretreated GSK2879552 (50 μM, 0.5 or 48 h). **a**, Overlap of AR peaks in treated cells. **b**, The heat map view of AR- and FOXA1-binding intensity at AR-binding sites. **c**, The mean of AR-binding intensity at AR-binding sites (Veh versus GSK-4 h: $P = 8.8 \times 10^{-33}$; Veh versus GSK-48 h: $P = 9.9 \times 10^{-267}$). **d**,**e**, ChIP–qPCR for AR (**d**) or p300 (**e**) at AR-mediated enhancers in LNCaP cells treated with/without DHT (10 nM, 4 h) and pretreated with GSK2879552 (48 h). **f**, RT–qPCR for *KLK3* in LNCaP cells treated with 1–10 nM DHT (24 h) and pretreated with GSK2879552 (0–50 μM, 24 h). **g**–**j**, LNCaP cells were maintained in the medium containing vehicle or 1 μM GSK2879552 for ~2 weeks (2 w). The following experiments were performed: RT–qPCR for *KLK3* (**g**); immunoblotting for KLK3 (**h**); ChIP–qPCR for FOXA1 binding (**i**); ChIP–qPCR for AR binding (with 10 nM DHT) (**j**). **k**, RNA-seq analyses were done in these long-term GSK2879552-treated cells (10 nM DHT, 24 h) in comparison with parental LNCaP cells pretreated with 50 μM GSK2879552 (24 h) and treated with/without DHT (10 nM, 24 h). Androgen-upregulated genes were identified from parental LNCaP cells by using twofold cut-off (DHT/Veh). The heat map view for the change in expression in response to GSK2879552 treatment is shown. **l**, Cell density was examined under the indicated conditions (mean ± s.d.). **m**, LNCaP cells stably expressing doxycycline (Dox)-inducible AR-V7 (V5 tagged) (LNCaP-tetARV7) were subjected to immunoblotting. **n**, ChIP–qPCR for V5 binding in LNCaP-tetARV7 cells treated with doxycycline versus doxycycline plus GSK2879552 (10 μM, 24 h). **o**, RT–qPCR for AR-V7-regulated genes in these cells. **p**, ChIP–qPCR for AR-V7 binding in CWR22-RV1 cells treated with GSK2879552 (2.5 μM, 24 h). **q**, ChIP–qPCR for AR-V7 binding in the LSD1-KO line versus the control line.

(Fig. 2f and Extended Data Fig. 4i). Interestingly, the prolonged treatment of LSD1 inhibitor (~2 weeks) at much lower doses (1 μM) can recapitulate the effect of higher doses of inhibitor (50 μM for 48 h) on FOXA1/AR chromatin binding, AR transcriptional activity and PCa cell growth (Fig. 2g–l and Extended Data Fig. 4j), suggesting that the effect of LSD1-inhibitor treatment is sustainable and accumulative. Genes repressed or enhanced by the short-term or prolonged treatment were also similarly enriched for unfolded protein responses or immune responses, respectively (Extended Data Fig. 4k). The latter functions were also reported in a recent study showing that LSD1 ablation enhances antitumor immunity[21].

We next sought to determine whether LSD1 inhibition affects chromatin binding of the constitutively active form of AR splice variants lacking the ligand-binding domain (such as AR-V7, NM_001348061.1)[22–24]. As shown in Fig. 2m–q and Extended Data Fig. 5a–e, LSD1 inhibition or silencing decreased ligand-independent AR-V7 chromatin binding and its transcriptional activity in either AR-V7-overexpressing LNCaP cells or in CWR22-RV1 cells (with high levels of endogenous AR-V7 (refs. [25,26])) without noticeably affecting AR-V7 protein expression. Overall, these results demonstrate that AR signaling is suppressed by LSD1 inhibition through globally impairing the chromatin recruitment of AR and AR splice variants.

In addition to its classic function of demethylating H3K4, LSD1 can also demethylate nonhistone proteins[27–29]. Since LSD1 physically interacts with FOXA1 (refs. [11,30]), we hypothesized that LSD1 may regulate FOXA1 binding through the demethylation of FOXA1. As seen in Fig. 3a and Extended Data Fig. 6a,b, the levels of lysine-methylated FOXA1 were increased by LSD1 inhibitors and decreased by overexpression of LSD1-WT, but not the K661A mutant. A mass spectrometry analysis was then performed on the immunopurified FOXA1, leading to identification of methylated lysine 270 (K270me) as a potential substrate of LSD1 (Extended Data Fig. 6c). This residue resides at the carboxyl end of the wing2 region (amino acids 247–269) of the Forkhead DNA-binding domain, a hotspot region for recurrent FOXA1 mutations in PCa[31–36] (Fig. 3b), and was recently reported as a critical residue for FOXA1 interaction with the nucleosome core[37]. The demethylase activity of LSD1 on FOXA1 peptide containing K270me was subsequently determined and validated (Fig. 3c,d). Moreover, the level of lysine-methylated FOXA1 was noticeably reduced in cells expressing methylation-deficient mutant K270R, suggesting that K270 is a major methylation site (Fig. 3e). We then generated a FOXA1-K270me-specific antibody to confirm LSD1-mediated demethylation in PCa cells. As seen in Fig. 3f, K270me was only detected in immunoprecipitated FOXA1-WT, but not the K270R mutant, and its level was increased by LSD1 inhibition, confirming that K270me is demethylated by LSD1 in vivo. In contrast to the suppression effect on FOXA1-WT, LSD1 inhibition or depletion did not decrease the chromatin binding of FOXA1-K270R at AR-regulated enhancers (Fig. 3g and Extended Data Fig. 6d–g).

We next sought to determine the role of K270me on FOXA1 chromatin binding and the subsequent recruitment of AR. Using biochemical fractionation assays, we show that the K270R mutant was more tightly associated with chromatin (Extended Data Fig. 7a,b). Moreover, K270R-expressing cells contained substantially more FOXA1-binding sites and higher binding intensity than WT-expressing cells and were less affected by LSD1 inhibition (~30% loss versus ~51% loss with WT) (Fig. 3h–i), indicating that K270me may disrupt FOXA1 binding to chromatin. Notably, overexpressing the K270R mutant resulted in a global increase in AR recruitment to chromosomes (Fig. 3j and Extended Data Fig. 7c). Moreover, AR recruitment and activity in FOXA1-K270R cells were more resistant to a potent AR antagonist, enzalutamide[38], and overexpressing the K270R mutant resulted in enzalutamide resistance in AR-mediated PCa tumor growth (Fig. 3k–m and Extended Data Fig. 7d,e), indicating that K270me may further impair AR recruitment and increase its sensitivity to the antagonist treatment. Overall, these results indicate that LSD1-mediated K270 demethylation stabilizes FOXA1 binding and enhances the chromatin recruitment of AR.

The Forkhead DNA-binding domain is conserved within members of FOXA proteins. As seen in Extended Data Fig. 8a, FOXA2 shares the same sequence of wing2 loop and the lysine adjacent to it (K265). Therefore, we hypothesized that FOXA2 chromatin binding may also be regulated by LSD1-mediated demethylation. In PCa, FOXA2 activity is linked to the small-cell neuroendocrine subtype[39] and it is expressed in AR-negative PC-3 cells (Extended Data Fig. 8b). Importantly, FOXA2 chromatin binding in PC-3 cells was suppressed by LSD1 inhibition while the chromatin binding of HOXB13, another important pioneer factor of AR[40], was not suppressed by LSD1 inhibition in LNCaP cells (Extended Data Fig. 8c–f), suggesting that LSD1-mediated demethylation is a specific mechanism regulating the chromatin binding of FOXA1/2.

FOXA1 is highly expressed in PCa, breast cancer and small-cell lung cancer, and its expression is correlated with LSD1 (Extended Data Fig. 9a–c). Several LSD1 inhibitors (GSK2879552, ORY-1001, INCB059872, SP2577) are being tested in clinical trials for cancer treatment[15,17,41,42]. To examine how FOXA1-positive castration-resistant PCa (CRPC) responds to LSD1 inhibition, we generated CWR22-RV1 xenograft tumors in castrated mice and treated them with GSK2879552. As shown in Fig. 4a, CWR22-RV1 tumor growth was markedly repressed by LSD1 inhibition, which led to an increase in H3K4me2 and a decrease in AR-FL/V7-regulated gene expression (Fig. 4b and Extended Data Fig. 9d–f). In contrast, LSD1 inhibition did not affect the growth of CWR22-RV1 tumors expressing the K270R mutant, indicating that the effect of LSD1-inhibitor treatment is mediated via blocking FOXA1 K270 demethylation (Fig. 4c).

To further determine whether FOXA1 expression affects the efficacy of LSD1 inhibitors in vivo, we established three additional CRPC xenograft models with various expression levels of FOXA1, including LuCaP35CR, LuCaP77CR[43,44] and DU145. LuCaP35CR tumors express high levels of FOXA1, whereas LuCaP77CR and DU145 tumors have a much weaker or undetectable expression of FOXA1, respectively (Fig. 4d). Similarly to the CWR22-RV1 model, LuCaP35CR tumors were very sensitive to GSK2879552 and ORY-1001, and these treatments suppressed FOXA1 chromatin binding and the expression of AR-FL/V7-regulated genes (Fig. 4e–g and Extended Data Fig. 10a–f). However, the tumor responses to the LSD1 inhibitor in the LuCaP77CR model were much weaker and the suppression of AR-FL/AR-V7 signaling was not significant, although this treatment can similarly increase H3K4me2 (Fig. 4h,i and Extended Data Fig. 10g). In sharp contrast to CWR22-RV1 and LuCaP35CR, LSD1 inhibition did not affect the growth of FOXA1-negative DU145 tumors (Fig. 4j and Extended Data Fig. 10h). Taken together, these in vivo animal studies suggest that the efficacy of LSD1-inhibitor treatment in CRPC may be correlated with the expression levels of FOXA1.

Finally, we examined whether LSD1-inhibitor treatment could therapeutically synergize with enzalutamide. As seen in Extended Data Fig. 10i, the additive effect of LSD1 inhibitor with enzalutamide on suppressing the growth of CWR22-RV1 cells was observed in cell culture. More importantly, treating the mice bearing CWR22-RV1 xenografts with GSK2879552 (at a lower dose) and enzalutamide noticeably increased the efficacy of the treatment by enzalutamide alone (Fig. 4k), indicating a therapeutic potential for combining LSD1 inhibitor with intense androgen-deprivation therapies to treat PCa.

In summary, these findings indicate that FOXA1 chromatin binding is regulated by LSD1-mediated demethylation at K270 and, with this mechanism, LSD1 maintains the enhancer accessibility

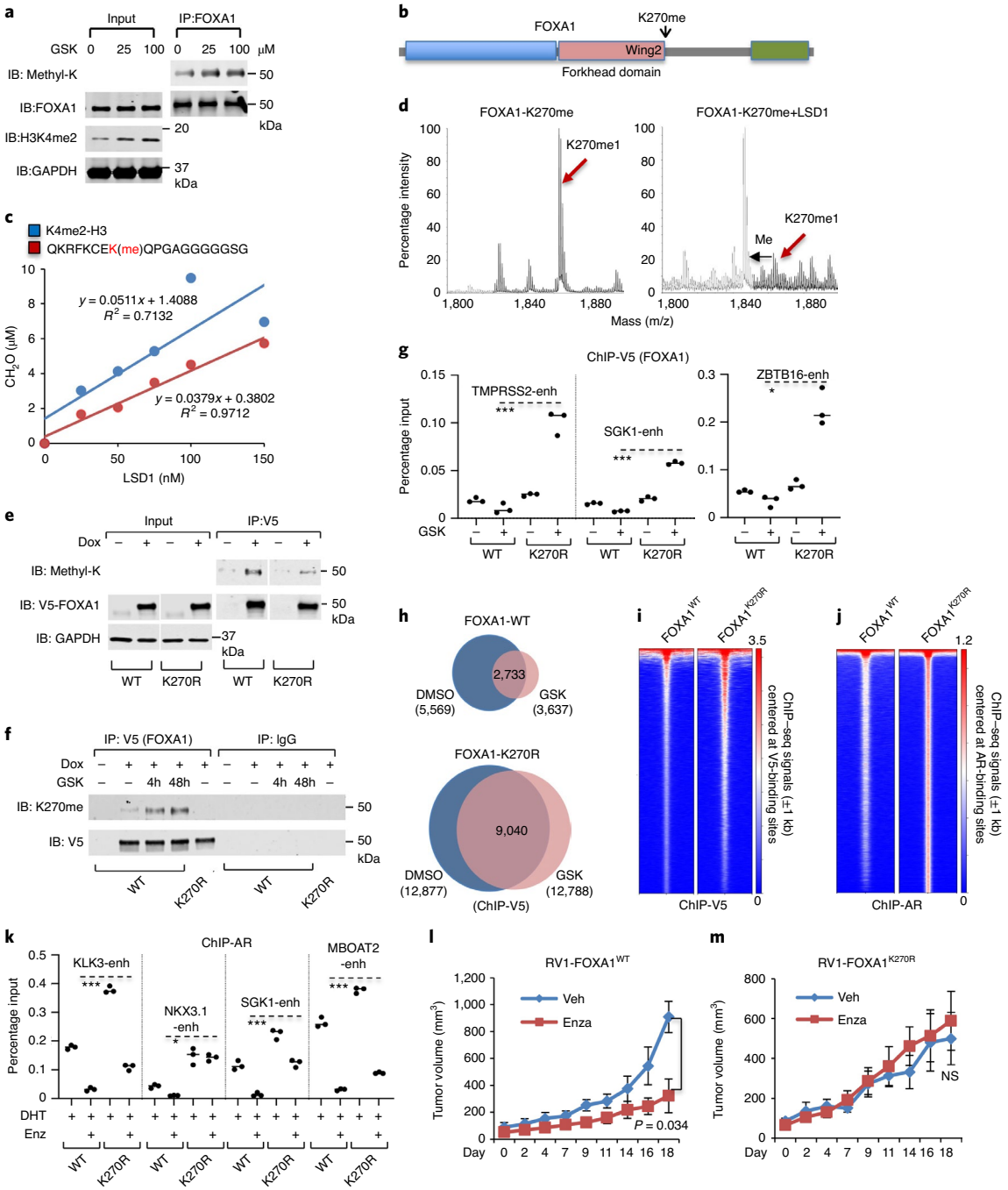

Fig. 3 | LSD1 regulates FOXA1 chromatin binding through directly demethylating its lysine 270. a, FOXA1 was immunoprecipitated (IP) from CWR22-RV1 cells treated with GSK2879552 (0–100 μM), followed by immunoblotting (IB) for methyl-lysine. **b**, Mass spectrometry analyses for immunoprecipitated FOXA1 from LNCaP cells stably overexpressing V5-FOXA1 identified methylated K270. **c**, The in vitro demethylation assay (measuring formaldehyde production) using synthetic H3K4me2 peptide (amino acids 1–21) or K270-methylated FOXA1 peptide (amino acids 263–281) as substrates and incubated with recombinant LSD1 protein. **d**, The K270-methylated FOXA1 peptide incubated with/without 75 nM LSD1 (1 h) was analyzed by mass spectrometry. 'Me' indicates a shift in mass equivalent to one methyl group. **e**, CWR22-RV1 cells stably expressing doxycycline-inducible V5-tagged FOXA1-WT or K270R (CWR22-RV1-tetFOXA1^{WT} or CWR22-RV1-tetFOXA1^{K270R} cells) were generated for the following experiments. Immunoblotting for methyllysine on immunopurified V5-FOXA1 is shown (images cropped from the same blot). **f**, Immunoblotting for K270-methylated FOXA1 on immunopurified V5-FOXA1 protein. **g**, ChIP–qPCR for FOXA1-WT or K270R binding at AR-regulated enhancers in these stable cells treated with GSK2879552 (24 h). **h**,**i**, V5 ChIP–seq analyses were performed in the stable cells treated with/without GSK2879552 (50 μM, 4 h). The Venn diagram for V5-binding peaks (**h**) and the heat map view for V5-FOXA1-binding intensity (vehicle treated) (**i**) are shown. **j**, AR ChIP–seq analyses were performed in these stable cells treated with DHT (10 nM, 4 h), and the heat map view for AR-binding intensity is shown. **k**, ChIP–qPCR for AR binding in these stable cells treated with DHT (10 nM) versus DHT plus enzalutamide (Enza, 10 μM). Note: cells in **g**–**k** were all grown in the doxycycline-supplemented hormone-depleted medium. **l**,**m**, SCID male mice bearing xenograft tumors established from WT (**l**) versus K270R mutant (**m**) expressing CWR22-RV1 stable cell lines were fed with doxycycline-supplemented diet and received daily enzalutamide treatment (10 mg kg^{-1}) via intraperitoneal injection ($n = 4$ independent tumors). The tumor volume (mean ± s.d.) was measured at the indicated time.

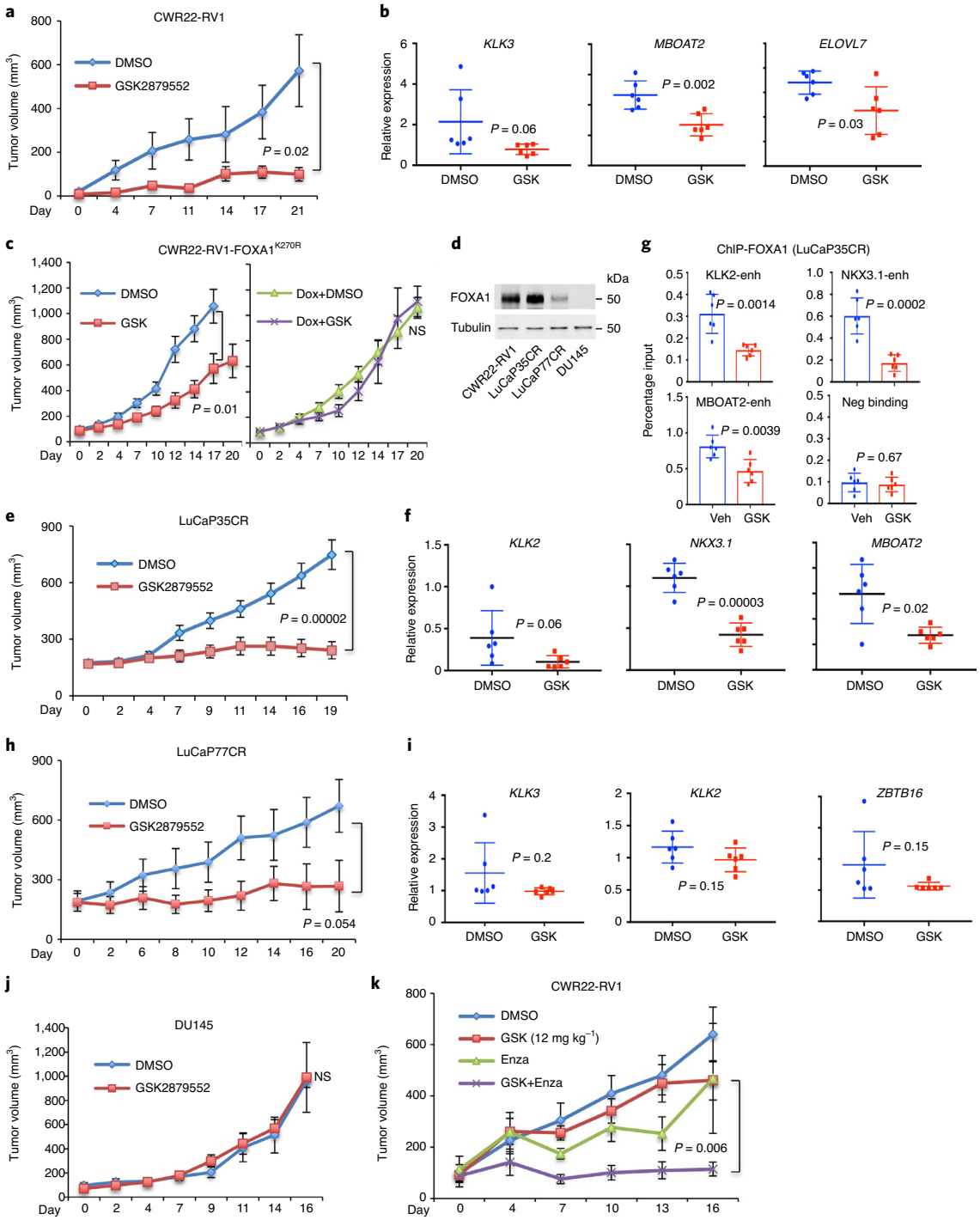

Fig. 4 | LSD1-inhibitor treatment suppresses tumor growth alone or in synergy with enzalutamide in FOXA1-high CRPC models. a,**b**, Castrated SCID male mice bearing CWR22-RV1 xenograft tumors received daily DMSO or GSK2879552 (33 mg kg^{-1}) via intraperitoneal injection (n = 6 independent tumors). **a**, The tumor growth was recorded. **b**, After the mice were killed, tumor samples were subjected to RT-qPCR for the indicated AR-FL/V7-regulated genes. **c**, Castrated SCID male mice bearing CWR22-RV1-tetFOXA1^{K270R} xenograft tumors fed with regular or doxycycline-supplemented diet were treated with daily DMSO or GSK2879552 (33 mg kg^{-1}) via intraperitoneal injection (n = 8 independent tumors). The tumor growth was recorded. **d**, The protein expression of FOXA1 was examined in tumor samples from vehicle-treated xenograft tumors of four CRPC models. **e**–**g**, Castrated SCID male mice bearing LuCaP35CR xenograft tumors received daily DMSO or GSK2879552 (33 mg kg^{-1}) via intraperitoneal injection (n = 12 independent tumors). The tumor growth was recorded (**e**) and the tumor samples were subjected to RT-qPCR for indicated AR-FL/V7-regulated genes (**f**) and ChIP-qPCR for FOXA1 binding at indicated sites (**g**). **h**,**i**, Castrated SCID male mice bearing LuCaP77CR xenograft tumors received daily DMSO or GSK2879552 (33 mg kg^{-1}) via intraperitoneal injection (n = 7 independent tumors). The tumor growth was recorded (**h**) and tumor samples were subjected to RT-qPCR for indicated AR-FL/V7-regulated genes (**i**). **j**, Castrated SCID male mice bearing DU145 xenograft tumors received daily DMSO or GSK2879552 (33 mg kg^{-1}) via intraperitoneal injection (n = 6 independent tumors). **k**, SCID mice bearing CWR22-RV1 xenograft tumors received daily DMSO, GSK2879552 (12 mg kg^{-1}), enzalutamide (10 mg kg^{-1}) or the combination via intraperitoneal injection (n = 6 independent tumors). Note: the statistical difference for the tumor growth (mean ± s.d.) at the final time point was determined by a two-tailed Student's t-test.

to AR (and other steroid hormone receptors) and thus regulates its chromatin binding and transcriptional output. It is now well accepted that AR remains a major driver of CRPC that relapses after castration therapies and treatments with abiraterone or enzalutamide[38,45]. Importantly, recent studies revealed that a substantial portion of CRPC patient samples (~25%) contain chromatin rearrangements within a FOXA1 enhancer, which drive the overexpression of FOXA1 and the restoration of AR signaling[35]. Therefore, there is a critical need for developing approaches and agents to target FOXA1 through novel mechanisms, and LSD1 inhibition is an attractive approach to inhibit the FOXA1-AR axis in CRPC. Our findings also suggest that LSD1 inhibition is a promising therapeutic strategy to suppress the activity of the constitutively active AR splice variants, as it directly targets the chromatin binding of these AR variants. With more active and selective LSD1 inhibitors being developed and tested in the clinic, these preclinical findings may pave the way to improve treatment of PCa patients with FOXA1 overexpression.

Online content

Any methods, additional references, Nature Research reporting summaries, source data, extended data, supplementary information, acknowledgements, peer review information; details of author contributions and competing interests; and statements of data and code availability are available at https://doi.org/10.1038/s41588-020-0681-7.

Received: 1 May 2018; Accepted: 24 July 2020;
Published online: 31 August 2020

References

1. Gao, N. et al. The role of hepatocyte nuclear factor-3 alpha (forkhead box A1) and androgen receptor in transcriptional regulation of prostatic genes. *Mol. Endocrinol.* **17**, 1484–1507 (2003).
2. Carroll, J. S. et al. Chromosome-wide mapping of estrogen receptor binding reveals long-range regulation requiring the forkhead protein FoxA1. *Cell* **122**, 33–43 (2005).
3. Jozwik, K. M. & Carroll, J. S. Pioneer factors in hormone-dependent cancers. *Nat. Rev. Cancer* **12**, 381–385 (2012).
4. Yang, Y. A. & Yu, J. Current perspectives on FOXA1 regulation of androgen receptor signaling and prostate cancer. *Genes Dis.* **2**, 144–151 (2015).
5. Shi, Y. et al. Histone demethylation mediated by the nuclear amine oxidase homolog LSD1. *Cell* **119**, 941–953 (2004).
6. Shi, Y. J. et al. Regulation of LSD1 histone demethylase activity by its associated factors. *Mol. Cell* **19**, 857–864 (2005).
7. Metzger, E. et al. LSD1 demethylates repressive histone marks to promote androgen-receptor-dependent transcription. *Nature* **437**, 436–439 (2005).
8. Wissmann, M. et al. Cooperative demethylation by JMJD2C and LSD1 promotes androgen receptor-dependent gene expression. *Nat. Cell Biol.* **9**, 347–353 (2007).
9. Metzger, E. et al. Phosphorylation of histone H3 at threonine 11 establishes a novel chromatin mark for transcriptional regulation. *Nat. Cell Biol.* **10**, 53–60 (2008).
10. Metzger, E. et al. Phosphorylation of histone H3T6 by PKCβ_1 controls demethylation at histone H3K4. *Nature* **464**, 792–796 (2010).
11. Cai, C. et al. Lysine-specific demethylase 1 has dual functions as a major regulator of androgen receptor transcriptional activity. *Cell Rep.* **9**, 1618–1627 (2014).
12. Lupien, M. et al. FoxA1 translates epigenetic signatures into enhancer-driven lineage-specific transcription. *Cell* **132**, 958–970 (2008).
13. Swinstead, E. E. et al. Steroid receptors reprogram FoxA1 occupancy through dynamic chromatin transitions. *Cell* **165**, 593–605 (2016).
14. Metzger, E. et al. Assembly of methylated KDM1A and CHD1 drives androgen receptor-dependent transcription and translocation. *Nat. Struct. Mol. Biol.* **23**, 132–139 (2016).
15. Sehrawat, A. et al. LSD1 activates a lethal prostate cancer gene network independently of its demethylase function. *Proc. Natl Acad. Sci. USA* **115**, E4179–E4188 (2018).
16. Mimasu, S. et al. Structurally designed *trans*-2-phenylcyclopropylamine derivatives potently inhibit histone demethylase LSD1/KDM1. *Biochemistry* **49**, 6494–6503 (2010).
17. Mohammad, H. P. et al. A DNA hypomethylation signature predicts antitumor activity of LSD1 inhibitors in SCLC. *Cancer Cell* **28**, 57–69 (2015).
18. He, H. H. et al. Differential DNase I hypersensitivity reveals factor-dependent chromatin dynamics. *Genome Res.* **22**, 1015–1025 (2012).
19. Wang, D. et al. Reprogramming transcription by distinct classes of enhancers functionally defined by eRNA. *Nature* **474**, 390–394 (2011).
20. Jin, H. J., Zhao, J. C., Wu, L., Kim, J. & Yu, J. Cooperativity and equilibrium with FOXA1 define the androgen receptor transcriptional program. *Nat. Commun.* **5**, 3972 (2014).
21. Sheng, W. et al. LSD1 ablation stimulates anti-tumor immunity and enables checkpoint blockade. *Cell* **174**, 549–563.e19 (2018).
22. Antonarakis, E. S. et al. AR-V7 and resistance to enzalutamide and abiraterone in prostate cancer. *N. Engl. J. Med.* **371**, 1028–1038 (2014).
23. Yu, Z. et al. Rapid induction of androgen receptor splice variants by androgen deprivation in prostate cancer. *Clin. Cancer Res.* **20**, 1590–1600 (2014).
24. Sharp, A. et al. Androgen receptor splice variant-7 expression emerges with castration resistance in prostate cancer. *J. Clin. Invest.* **129**, 192–208 (2019).
25. Hu, R. et al. Ligand-independent androgen receptor variants derived from splicing of cryptic exons signify hormone-refractory prostate cancer. *Cancer Res.* **69**, 16–22 (2009).
26. Li, Y. et al. Intragenic rearrangement and altered RNA splicing of the androgen receptor in a cell-based model of prostate cancer progression. *Cancer Res.* **71**, 2108–2117 (2011).
27. Huang, J. et al. p53 is regulated by the lysine demethylase LSD1. *Nature* **449**, 105–108 (2007).
28. Wang, J. et al. The lysine demethylase LSD1 (KDM1) is required for maintenance of global DNA methylation. *Nat. Genet.* **41**, 125–129 (2009).
29. Kontaki, H. & Talianidis, I. Lysine methylation regulates E2F1-induced cell death. *Mol. Cell* **39**, 152–160 (2010).
30. Jozwik, K. M., Chernukhin, I., Serandour, A. A., Nagarajan, S. & Carroll, J. S. FOXA1 directs H3K4 monomethylation at enhancers via recruitment of the methyltransferase MLL3. *Cell Rep.* **17**, 2715–2723 (2016).
31. Barbieri, C. E. et al. Exome sequencing identifies recurrent SPOP, FOXA1 and MED12 mutations in prostate cancer. *Nat. Genet.* **44**, 685–689 (2012).
32. Grasso, C. S. et al. The mutational landscape of lethal castration-resistant prostate cancer. *Nature* **487**, 239–243 (2012).
33. Cancer Genome Atlas Research Network. The molecular taxonomy of primary prostate cancer. *Cell* **163**, 1011–1025 (2015).
34. Robinson, D. et al. Integrative clinical genomics of advanced prostate cancer. *Cell* **161**, 1215–1228 (2015).
35. Parolia, A. et al. Distinct structural classes of activating FOXA1 alterations in advanced prostate cancer. *Nature* **571**, 413–418 (2019).
36. Li, J. et al. A genomic and epigenomic atlas of prostate cancer in Asian populations. *Nature* **580**, 93–99 (2020).
37. Iwafuchi, M. et al. Gene network transitions in embryos depend upon interactions between a pioneer transcription factor and core histones. *Nat. Genet.* **52**, 418–427 (2020).
38. Scher, H. I. et al. Increased survival with enzalutamide in prostate cancer after chemotherapy. *N. Engl. J. Med.* **367**, 1187–1197 (2012).
39. Park, J. W., Lee, J. K., Witte, O. N. & Huang, J. FOXA2 is a sensitive and specific marker for small cell neuroendocrine carcinoma of the prostate. *Mod. Pathol.* **30**, 1262–1272 (2017).
40. Brechka, H., Bhanvadia, R. R., VanOpstall, C. & Vander Griend, D. J. HOXB13 mutations and binding partners in prostate development and cancer: function, clinical significance, and future directions. *Genes Dis.* **4**, 75–87 (2017).
41. Maes, T. et al. ORY-1001, a potent and selective covalent KDM1A inhibitor, for the treatment of acute leukemia. *Cancer Cell* **33**, 495–511.e12 (2018).
42. Pishas, K. I. et al. Therapeutic targeting of KDM1A/LSD1 in Ewing sarcoma with SP-2509 engages the endoplasmic reticulum stress response. *Mol. Cancer Ther.* **17**, 1902–1916 (2018).
43. Corey, E. et al. LuCaP 35: a new model of prostate cancer progression to androgen independence. *Prostate* **55**, 239–246 (2003).
44. Nguyen, H. M. et al. LuCaP prostate cancer patient-derived xenografts reflect the molecular heterogeneity of advanced disease and serve as models for evaluating cancer therapeutics. *Prostate* **77**, 654–671 (2017).
45. de Bono, J. S. et al. Abiraterone and increased survival in metastatic prostate cancer. *N. Engl. J. Med.* **364**, 1995–2005 (2011).

Methods

Cell culture and viral transduction. LNCaP, CWR22-RV1, DU145 and PC-3 cells were purchased from ATCC and cultured in RPMI 1640 with 10% FBS. All lines were authenticated using short tandem repeat profiling and tested for mycoplasma contamination (MycoAlert kit, Lonza) every 6 months. MCF-7 cells were kindly gifted by X. Yuan at Beth Israel Deaconess Medical Center and were cultured in DMEM with 10% FBS. For androgen-stimulation assays, cells were grown to 50%–60% confluence in medium containing 5% CSS for 2–3 d and then treated with DHT for 0–48 h. Short interfering RNAs (siRNA) against *FOXA1* or *LSD1* were obtained from Dharmacon RNAi Technologies (ON-TARGETplus).

Entry vectors of FOXA1 and LSD1 were purchased from the PlasmID Repository of Harvard Medical School. pLIX_403 lentiviral vectors for expression of FOXA1-WT, FOXA1-K270R, LSD1-WT or LSD1-K661A were generated using the Gateway Technology with Clonase II (Invitrogen, catalog no. 12535-029). FOXA1-K270R point mutation (A>G) and LSD1-K661A (A>G, A>C) were generated using the QuickChange Lightning Site-Directed Mutagenesis Kit (Agilent Technologies) according to the manufacturer's protocol. The primers for generating FOXA1-K270R and LSD1-K661A are listed in Supplementary Table 1. Lentiviral particles were assembled in HEK293T cells by using the 2nd generation system. In brief, 3 d after transfection in HEK293T cells, viral supernatant was centrifuged for 10 min at 3,000 r.p.m. to remove any cell debris and passed through a 0.45-μm filter. The collected lentiviral particles were used to infect the cells in the presence of polybrene, followed by selection with puromycin (Gibco).

Generation of CRISPR knockout clones. Lentivirus for expression of Cas9 (lentiCas9-Blast; Addgene, catolog no. 52962) was assembled by using an approach similar to that mentioned above. CWR22-RV1 cells stably expressing Cas9 were first generated by infection of lentiCas9 through selection of blasticidin. Cas9 expression was confirmed by immunoblotting (Abcam, catalog no. 210752). CWR22-RV1–Cas9 cells were then transiently transfected using Lipofectamine 2000 (Thermo Fisher) with lentiCRISPR-V2 (Addgene, catalog no. 52961) for expression of sgLSD1 (5′-GGGGCCTGGCGGAACCGCCG-3′), which was described in a previous study[21]. Cells were then selected by puromycin until single-cell clones emerged. Individual clones were further expanded and the loss of LSD1 expression was confirmed by immunoblotting.

In vitro demethylation assay. Formaldehyde production was measured using the Histone Demethylase Assay kit (Active Motif) following the manufacturer's protocol. Synthetic FOXA1 peptide (amino acids 263–281) (GenScript, with >98% purity) or H3K4me2 (amino acids 1–21) peptide (Active Motif) were incubated with 0–150 nM recombinant LSD1 (Active Motif) in demethylation buffer for 1 h at 37 °C, and then detection buffer for 1 h at 37 °C, followed by fluorescence detection with excitation wavelength at 410 nm and emission wavelength at 480 nm. The reaction mixture was further analyzed by matrix-assisted laser desorption/ionization mass spectrometry at the Molecular Biology Core of Dana-Farber Cancer Institute.

Immunoprecipitation and mass spectrometry. For endogenous FOXA1 immunoprecipitation, cells were lysed using RIPA lysis buffer (150 mM NaCl, 1% NP-40, 0.5% sodium deoxycholate, 0.1% SDS and 50 mM Tris pH 8.0) supplemented with protease inhibitors (Thermo Fisher), followed by preclearing using IgG-conjugated beads (Sigma) for 1 h at 4 °C. Equal amounts of protein (1–5 mg) were mixed with 25 μl anti-FOXA1-conjugated beads (Santa Cruz) overnight. Immunocomplexes were eluted with the sample buffer (Bio-Rad). For V5 pulldown, cells stably expressing doxycycline-induced V5-tagged FOXA1 were pretreated with doxycycline for 2 d, followed by GSK2879552 (50 μM) treatment for 16 h. Extracts were incubated with 15 μl anti-V5-conjugated beads overnight. For mass spectrometry, at least 6×10^8 cells were used for mapping the posttranslational modification sites through Thermo Orbitrap Elite and Thermo QExactive HF Orbitrap microcapillary liquid chromatography–mass spectrometry (LC–MS/MS) at the Mass Spectrometry Core of Beth Israel Deaconess Medical Center.

Chromatin immunoprecipitation. Cells were treated with S2101 (Calbiochem), OG-L002 (Selleckchem), C12 (XcessBio), GSK2879552 (Selleck) and 10 nM of DHT. ChIP assay was performed based on the previously described protocol[46]. Cells were cross-linked with 1% formaldehyde for 10 min and quenched by 125 mM glycine for 5 min at room temperature with gentle shaking. Cells were quickly rinsed in cold PBS twice and collected in PBS supplemented with protease inhibitors. Cells were then centrifuged and lysed in ice-cold lysis buffer (1% SDS, 5 mM EDTA, 50 mM Tris–HCl pH 8.1) supplemented with protease inhibitors for 10 min. The cell lysate was sonicated using a Bioruptor Sonicator (Diagenode) to break DNA into ~300-base pair (bp) fragments (~500 bp for ChIP–quantitative PCR (qPCR)). Soluble chromatin was diluted in dilution buffer (1% Triton X-100, 2 mM EDTA, 150 mM NaCl, 20 mM Tris–HCl pH 8.1), and 4 μg ChIP-grade antibody was added and incubated at 4 °C overnight with gentle shaking. A 50-μl protein A or G beads flurry with yeast RNA (final concentration 100 μg ml^{-1}) (Thermo Fisher) was added and incubated for 1 h at 4 °C. The beads were then washed in the following buffers for 10 min each at 4 °C: TSE I (0.1% SDS, 1% Triton X-100, 2 mM EDTA, 150 mM NaCl, 20 mM Tris–HCl pH 8.1), TSE II (0.1% SDS, 1% Triton X-100, 2 mM EDTA, 500 mM NaCl, 20 mM Tris–HCl pH 8.1), Buffer III (0.25 mM LiCl, 1% NP-40, 1% deoxycholate, 1 mM EDTA, 10 mM Tris–HCl pH 8.1) and TE buffer (two times). To elute DNA, beads were incubated in elution buffer (1% SDS, 0.1 M $NaHCO_3$) at room temperature with aggressive shaking for 15 min. The supernatant was then collected and incubated at 65 °C overnight to reverse-cross-link the DNA. Qiagen QIAquick Purification Kit was used for purifying the DNA for subsequent sequencing or PCR approaches. For ChIP assay using tumor tissues, ~20 mg of frozen tissue sample was cut into small pieces and homogenized by handheld TissueRuptor II (Qiagen). Cells were washed in cold PBS two times and centrifuged. The cell pellet was resuspended in PBS supplemented with protease inhibitors and then incubated with formaldehyde (final concentration of 1%) at room temperature for 10 min. The rest of the steps are the same as for the ChIP assay using culture cells. The following antibodies were used in ChIP: anti-FOXA1 antibody no. 1 (Abcam, catalog no. ab23738), anti-FOXA1 antibody no. 2 (Abcam, catalog no. ab5089), anti-FOXA2 antibody (Millipore, catalog no. 17-10258), anti-HOXB13 antibody (Cell Signaling, catalog no. 90944), anti-H3K4me2 antibody (Millipore, catalog no. 07-030), anti-H3K27ac antibody (Abcam, catalog no. ab4729), anti-AR antibody (Santa Cruz, catalog no. sc-815), anti-V5 (Thermo Fisher, catalog no. R960-25), anti-AR-V7 (Precision Antibody, catalog no. AG10008), anti-p300 (Abcam, catalog no. ab10485) and anti-IgG (catalog no. 12-370, Millipore). The qPCR analysis was carried out using the SYBR Green method on the QuantStudio 3 Real-time PCR system (Thermo Fisher Scientific). ChIP–qPCR experiments were done in triplicate from independent tissue culture and the results were normalized to the input DNA.

For ChIP–seq analysis, library construction was prepared using ThruPLEX DNA-seq 48D Kit (Rubicon Genomics) based on the manufacturer's protocol, and the sequencing was performed on a HiSeq 2500 Illumina Genome Analyzer. Individual ChIP–seq was performed in technical duplicate and the raw data were merged for further analysis. All the detailed descriptions for ChIP–seq and other experiments can be found in the Life Sciences Reporting Summary.

ATAC–seq. Omni ATAC–seq was performed following a previously described protocol[47]. About 50,000 viable LNCaP cells (growing in 5% CSS) after GSK2879552 treatment were centrifuged at 500 relative centrifugal force at 4 °C. The pellet was lysed in 50 μl cold resuspension buffer (10 mM Tris–HCl pH 7.4, 10 mM NaCl, 3 mM $MgCl_2$ 0.1% NP-40, 0.1% Tween-20, and 0.01% Digitonin). The lysis solution was then diluted with 1 ml cold buffer (10 mM Tris–HCl pH 7.4, 10 mM NaCl, 3 mM $MgCl_2$, 0.1% Tween-20). Nuclei were collected by centrifugation at 500 relative centrifugal force at 4 °C for 10 min. The pellet was resuspended in 50 μl of transposition mixture (25 μl 2× TD buffer, 2.5 μl transposase, 16.5 μl PBS, 0.5 μl 1% digitonin, 0.5 μl 10% Tween-20, 5 μl H_2O) using an Illumina Tagment DNA TDE1 Enzyme and Buffer Kit, and incubated at 37 °C for 30 min in a thermomixer with 1,000 r.p.m. mixing. DNA samples were cleaned immediately with a Qiagen QIAquick Purification Kit and PCR preamplified by NEBNext High-Fidelity 2× PCR Master Mix. qPCR amplification was used to determine the additional cycles to prevent overamplification. The final PCR product was purified by Qiagen QIAquick Purification Kit and run on Agilent High Sensitivity Screen Tape for quality control. The libraries were sequenced on a HiSeq 2500 Illumina Genome Analyzer.

PCR with reverse transcription (RT–PCR) and RNA-seq. RNA was extracted with TRIzol Reagent (Invitrogen) based on the manufacturer's protocol. For tissue RNA isolation, the RNeasy Mini Kit (Qiagen) was used following the manufacturer's protocol. The same amounts of tissue samples were bead (5 mm) milled using a TissueLyser LT (Qiagen). Gene expression was measured using real-time RT–PCR analyses with TaqMan one-step RT–PCR reagents on a QuantStudio 3 Real-time PCR system and results were normalized to coamplified *GAPDH*. For RNA-seq analysis, RNA was purified using RNeasy Mini Kit (Qiagen). TruSeq Strnd Total RNA LT (Illumina) was used for library construction based on the manufacturer's protocol, and sequencing was performed on a HiSeq 2500 Illumina Genome Analyzer.

Subcellular fractionation assay. Subcellular Protein Fractionation Kit (Thermo Fisher) was used to extract the soluble nuclear fraction and chromatin-bound fraction. The number of cells used for the fractionation was 2×10^6 cells. After collecting cells with trypsin digestion, the following fractionations were isolated according to the manufacturer's protocol: the cytoplasmic extract was isolated using CEB buffer, the membrane extract was isolated using MEB buffer, the soluble nuclear extract was isolated using NEB buffer, the chromatin-bound extract was isolated using NEB buffer plus Micrococcal Nuclease and the cytoskeletal extract was isolated using PEB buffer. The extracts were boiled with 4× Laemmli buffer at 95 °C for 10 min before loading for immunoblotting.

Immunoblotting. Cells were lysed with RIPA buffer with protease inhibitors. For tissue protein isolation, tissue samples were bead (5 mm) milled in RIPA buffer with protease inhibitors by TissueLyser LT (Qiagen). Protein concentration was measured using the Pierce BCA Protein Assay Kit. Samples with the same volume and amount of protein were loaded in~4–15% Mini-PROTEAN TGX precast protein gels (Bio-Rad) and transferred to nitrocellulose membrane

(Bio-Rad). Membranes were blocked in 5% nonfat milk and incubated with the following antibodies at 4 °C overnight: anti-AR (Millipore, 1:1,000), anti-histone H3 (1:5,000), anti-H3K4me2 (1:1,000), anti-methyllysine (1:200), anti-LSD1 (1:1,000), anti-FOXA1 (1:2,000), anti-β-tubulin (1:5,000), anti-v5 (1:1,000), anti-GAPDH (1:5,000) (Abcam), anti-FOXA2 (1:1,000) (Millipore) and anti-KLK3 (1:1,000) (Meridian Life Science). The anti-FOXA1-K270me antibody was specially developed by Abcam. The company employed a phage library by using a 'Rapid Liquid Screening' approach (target sequence for selection: biotin-YLRRQKRFKCE(Kme1)QPGA). The antibody tested in the experiment is from the first round of IgG conversion (human/rabbit chimeric) based on the single-chain variable fragment resulting from screening. The antibody concentration used in immunoblotting was ~8 μg ml^{-1}. Membranes were then incubated with fluorescence-labeled secondary antibodies (LI-COR Biosciences) in 5% nonfat milk for 1 h at room temperature. Gel images were taken by the LI-COR Odyssey system at wavelengths of 680 or 800 nm. For detecting methylated FOXA1 with K270me-specific antibody, membranes were blocked in 5% BSA, and antibodies were diluted in 5% BSA (1:200). For detecting FOXA1 in FOXA1-immunoprecipitation experiments, EasyBlot secondary antibody (GeneTex) was used to eliminate the overlapping band of IgG heavy chain. Blots shown are representative of at least three independent experiments. The full scan of western blots can be found in the Source Data.

Cell counting. For testing prolonged inhibitor response, after treatments, cells were collected and fixed with 70% ethanol for 3 h, followed by staining with a Count & Viability Assay kit (proliferation) and cell counting with a Muse Cell Analyzer (EMD Millipore). For testing cell viability in response to different drug doses, CellTiter-Glo Luminescent Cell Viability Assay (Promega) was used. A total of 20,000 cells were seeded in 96-well plates and Glo Reagent was added to each well with a 1:1 ratio relative to the volume of the medium. After mixing on an orbital shaker for 5 min, the plate was incubated at room temperature for another 10 min and the intensity of the luminescence signal was recorded.

Xenograft tumors. CWR22-RV1 and DU145 xenograft tumors were established by subcutaneous injection of 1×10^6 cells in 6-week-old castrated male SCID mice (Taconic). For passaging LuCaP35CR and LuCaP77CR tumors, fresh tumors were cut into small pieces (using sharp scissors) and were trypsinized for 30 min, followed by resuspending tumor cells in RPMI 1640 mixed with Matrigel (1:1) and subcutaneous injection in castrated male SCID mice. For inducing FOXA1 expression in xenograft tumors derived from CWR22-RV1 stable cells overexpressing WT or K270R FOXA1, mice were fed with mouse chow supplemented with doxycycline (Teklad Custom Diet). During the treatment period, tumor volume was measured by electronic manual caliper using the formula $L \times W^2/2$ (where L is length and W is width). All animal experiments were approved by the UMass Boston Institutional Animal Care and Use Committee and were performed following institutional and national (USA) guidelines. The housing conditions were ambient temperatures of 65–75 °F with 40–60% humidity and 12-h light/12-h dark cycle.

Analysis for ChIP–seq and ATAC–seq. Raw reads were aligned to hg19 using bwa (v.0.7.2)[48] with the aln function followed by samse. For bwa aln, the first 32 subsequences were used as seed with trimming parameter setting as 5 (-l 32 -q 5). Default parameters were used for bwa samse. The resulting sam files were converted to bam with samtools (v.0.1.18)[49]. MACS2 (v.2.1.2)[50] was used to call peaks on the bam files with fix-bimodal turned on and extend size set at 100 (--bw 250 --mfold 10 30 --fix-bimodal --extsize 100). The q-value cut-off for peak significance was set as 0.05 (--qvalue 0.05). bedGraph files containing signal per million reads produced from MACS2 were converted to bigwig files with ucsctool kit (v.315). Briefly, bedGraph files were sorted with bedSort, clipped with bedClip and finally converted using bedGraphToBigWig to bigwig.

For global chromatin binding and accessibility analyses, all ChIP–seq and ATAC–seq results were normalized to the same sequencing depths. A high correlation of above 0.9 was observed between duplicates for all ChIP–seq and ATAC–seq data. To measure differences between averaged profiles for ChIP–seq and ATAC–seq, the nonparametric Kolmogorov–Smirnov test was used to calculate one-sided P values using data from both replicates. The R package ChIPpeakAnno (v.3.10.1)[51] was used for analyzing peak intervals. The function findOverlapsOfPeaks was used to determine overlapping among two or more peak sets. The deepTools suite (v.2.4.1)[52] was used to extract and visualize signals from bigwig files. The function computeMatrix was used with reference-point mode to calculate scores for each genomic region. Missing data were treated as zeros and regions with only zero values were skipped. The plotHeatmap and plotProfile functions were used to generate the heat map or a profile plot for scores over genomic regions.

RNA-seq analysis. Raw reads of RNA-seq were aligned to the hg19 reference genome using STAR (v.2.4.2a)[53] with gene counting function enabled (--quantMode GeneCounts). The infer_experiment.py function from RSeQC (v.2.6.1)[54] was used to determine how and whether the reads were stranded. Gene-level count data were then pulled according to the strandness information from the STAR output. Normalized counts per million were calculated before downstream analysis and a pseudo count of 1 was added when calculating fold change.

Target prediction. Binding and Expression Target Analysis (BETA v.1.0.7)[55] was used to predict targets from ChIP–seq and RNA-seq data. Peak interval files from MACS2 and differential analysis results from edgeR were used as input with the default parameter setting in running BETA.

Statistics and reproducibility. All ChIP–qPCR and qRT–PCR data were presented as the dot-plot format from samples collected from three independent tissue cultures. Statistical analysis was performed using unpaired two-tailed Student's t-test by comparing treatment versus vehicle control, or otherwise as indicated. We use NS ($P > 0.05$), *$0.001 < P < 0.01$, **$0.01 < P < 0.05$ and ***$P < 0.001$ to indicate the levels of P values in the main figures. For ChIP–seq and ATAC–seq results, the nonparametric Kolmogorov–Smirnov test was used to calculate one-sided P values using data from both replicates. For animal studies, a two-tailed Student's t-test was performed to determine the statistical difference of tumor growth at the final time point. The results for immunoblotting are representative of at least three biologically independent experiments. All statistical analyses and visualization were performed by using GraphPad (Prism 7/8) or R (v.3.4.0) unless otherwise specified.

PCR primers. For ChIP–qPCR, primers for KLK3-enh, KLK2-enh, NKX3.1-enh, SGK1-enh, SGK3-enh, MBOAT2-enh, RAB11B-FBS, PDK4-FBS and CDK1-FBS are listed in Supplementary Table 1. Primers for TMPRSS2-enh, ZBTB16-enh and SH2B1-enh were described previously[11]. Primers for TFF1-enh, NRIP1-enh, PGR-enh and DSCAM-enh were described previously[56,57].

For RT–qPCR, primer and probe sets for *KLK3* and *ZBTB16* are listed in Supplementary Table 1. Primer and probe sets for *MBOAT2* (Hs01027245_m1), *ELOVL7* (Hs00405151_m1), *FKBP5* (Hs01561006_m1), *NKX3.1* (Hs00171834_m1), *SGK1* (Hs00178612_m1), *ACSL3* (Hs00244853_m1), *ELOVL5* (Hs01094711_m1), *NANS* (Hs00219054_m1) and *AR-V7* (AI6R0CI) were purchased from Thermo Fisher.

Reporting Summary. Further information on research design is available in the Nature Research Reporting Summary linked to this article.

Data availability

All data generated or analyzed during this study are included in this published article. The GEO accession for ChIP–seq and RNA-seq data is GSE149007. Readers are welcome to comment on the online version of the paper. Correspondence and requests for materials should be addressed to C.C. (changmeng.cai@umb.edu). Source data are provided with this paper.

Code availability

This study did not generate any unpublished code, software or algorithm. All data analyses were performed using cited software with the parameters indicated in the Methods section.

References

46. Wang, Q. et al. Androgen receptor regulates a distinct transcription program in androgen-independent prostate cancer. *Cell* **138**, 245–256 (2009).
47. Corces, M. R. et al. An improved ATAC–seq protocol reduces background and enables interrogation of frozen tissues. *Nat. Methods* **14**, 959–962 (2017).
48. Li, H. Exploring single-sample SNP and INDEL calling with whole-genome de novo assembly. *Bioinformatics* **28**, 1838–1844 (2012).
49. Hsi-Yang Fritz, M., Leinonen, R., Cochrane, G. & Birney, E. Efficient storage of high throughput DNA sequencing data using reference-based compression. *Genome Res.* **21**, 734–740 (2011).
50. Zhang, Y. et al. Model-based analysis of ChIP-Seq (MACS). *Genome Biol.* **9**, R137 (2008).
51. Zhu, L. J. et al. ChIPpeakAnno: a Bioconductor package to annotate ChIP-seq and ChIP-chip data. *BMC Bioinformatics* **11**, 237 (2010).
52. Ramirez, F. et al. deepTools2: a next generation web server for deep-sequencing data analysis. *Nucleic Acids Res.* **44**, W160–W165 (2016).
53. Dobin, A. et al. STAR: ultrafast universal RNA-seq aligner. *Bioinformatics* **29**, 15–21 (2013).
54. Wang, L., Wang, S. & Li, W. RSeQC: quality control of RNA-seq experiments. *Bioinformatics* **28**, 2184–2185 (2012).
55. Wang, S. et al. Target analysis by integration of transcriptome and ChIP–seq data with BETA. *Nat. Protoc.* **8**, 2502–2515 (2013).
56. Hurtado, A., Holmes, K. A., Ross-Innes, C. S., Schmidt, D. & Carroll, J. S. FOXA1 is a key determinant of estrogen receptor function and endocrine response. *Nat. Genet.* **43**, 27–33 (2011).
57. Zhang, Y. et al. Nucleation of DNA repair factors by FOXA1 links DNA demethylation to transcriptional pioneering. *Nat. Genet.* **48**, 1003–1013 (2016).

Acknowledgements

This work is supported by grants from NIH (R00 CA166507 and R01 CA211350 to C.C., U54 CA156734 to C.C. and J.A.M. and P01 CA163227 to S.P.B.), DOD (W81XWH-15-1-0554 and W81XWH-19-1-0777 to S.G., W81XWH-16-1-0445 and W81XWH-19-1-0361 to C.C.), CIHR (142246, 152863, 152864 and 159567 to H.H.H.), Prostate Cancer Canada (RS2016-1022 and TAG2018-2061 to H.H.H.), NSERC (498706 to H.H.H.), Terry Fox Program Project Grants (1093 to H.H.H.) and Princess Margaret Cancer Foundation (to H.H.H.). H.H.H. holds a Joey and Toby Tanenbaum Brazilian Ball Chair in Prostate Cancer Research. We thank J. Asara and M. Yuan from Beth Israel Deaconess Medical Center and J. Lee from Dana-Farber Cancer Institute for the work on mass spectrometry analyses.

Author contributions

C.C., S.G., H.H.H., Sujun Chen and S.P.B. designed the study. S.G., Sujun Chen, D.H., Z.W., M. Li, W.H., A.B., M. Liu, F.Z., D.B., M.P.L., J.O., Y.L., M.A., J.P., E.C. and Sen Chen performed experiments and analyzed the results. S.P. and J.A.M. performed deep sequencing analyses. C.C., S.G., H.H.H., Sujun Chen and S.P.B. wrote the manuscript. All authors discussed the results and commented on the manuscript.

Competing interests

The authors declare no competing interests.

Additional information

Extended data is available for this paper at https://doi.org/10.1038/s41588-020-0681-7.

Supplementary information is available for this paper at https://doi.org/10.1038/s41588-020-0681-7.

Correspondence and requests for materials should be addressed to S.P.B., H.H.H. or C.C.

Reprints and permissions information is available at www.nature.com/reprints.

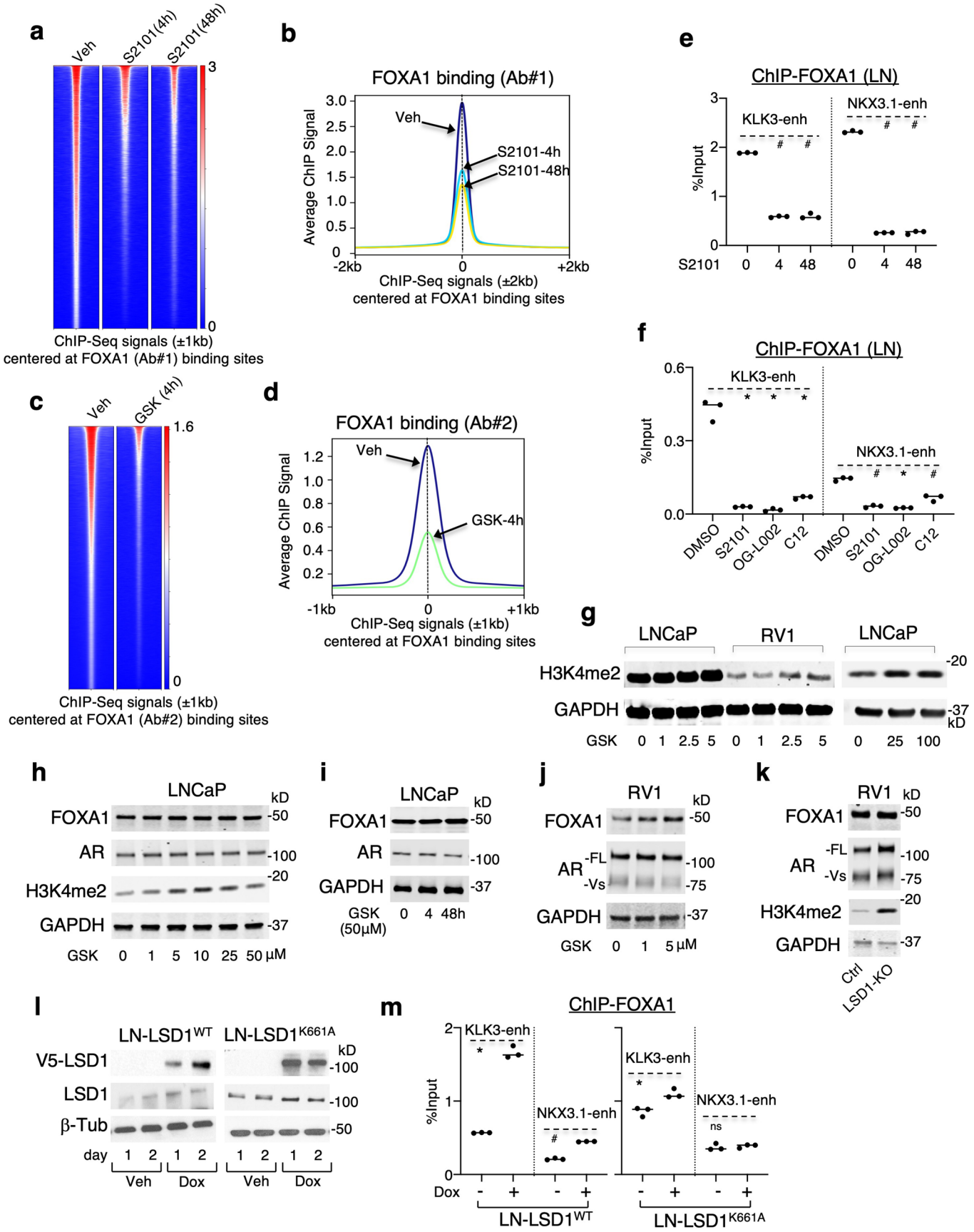

Extended Data Fig. 1 | See next page for caption.

Extended Data Fig. 1 | LSD1 promotes FOXA1 chromatin binding in PCa cells. a, **b**, FOXA1 ChIP-seq was performed using an anti-FOXA1 antibody (Ab no. 1) in LNCaP cells treated with vehicle or 50 μM S2101 for 4 hours (h) or 48 h. (**a**) The heatmap view for FOXA1 ChIP-seq peak intensity and (**b**) the mean of FOXA1 ChIP-seq signals at FOXA1 binding sites (Veh vs S2101-4 h: $P = 0.09$; Veh vs S2101-48 h: $P = 2.5 \times 10\text{-}5$) were shown. **c**, **d**, FOXA1 ChIP-seq was performed using an anti-FOXA1 antibody (Ab no. 2) in LNCaP cells treated with vehicle or GSK2879552 (50 μM, 4 h). (**c**) Heatmap view for FOXA1 ChIP-seq peak intensity and (**d**) the mean of FOXA1 ChIP-seq signals at FOXA1 binding sites (Veh vs GSK-4 h: $P = 7.0 \times 10^{-72}$) were shown. **e**, ChIP-qPCR for FOXA1 binding at *KLK3/NKX3.1* enhancer site. **f**, ChIP-qPCR for FOXA1 binding in LNCaP cells treated with vehicle or LSD1 inhibitors for 4 h (S2101, OG-L002 at 50 μM and C12 at 5 μM). **g**, Immunoblotting for H3K4me2 in LNCaP or CWR22-RV1 cells treated with GSK2879552 at indicated doses for 48 h. **h**, Immunoblotting for FOXA1 or AR in LNCaP cells treated with 0-50 μM GSK2879552 for 48 h. **i**, Immunoblotting for FOXA1 or AR in LNCaP cells treated with GSK2879552 (50 μM, 0-48 h). **j**, Immunoblotting for FOXA1 or AR in CWR22-RV1 cells treated with GSK2879552 (0-5 μM, 48 h). **k**, Immunoblotting for FOXA1 or AR in CWR22-RV1 control cell line versus LSD1-KO cell line. **l**, **m**, LNCaP cells stably overexpressing doxycycline (dox)-regulated LSD1-WT or LSD1-K661A mutant treated with/out doxycycline were subjected to (**l**) immunoblotting or (**m**) ChIP-qPCR for FOXA1 binding at indicated sites. Note: Experiments described in this figure were all done under hormone-depleted conditions. We use NS ($P > 0.05$), ^$0.01 < P < 0.05$, *$0.001 < P < 0.01$, and #$P < 0.001$) to indicate the levels of P value in all Extended Data Figures.

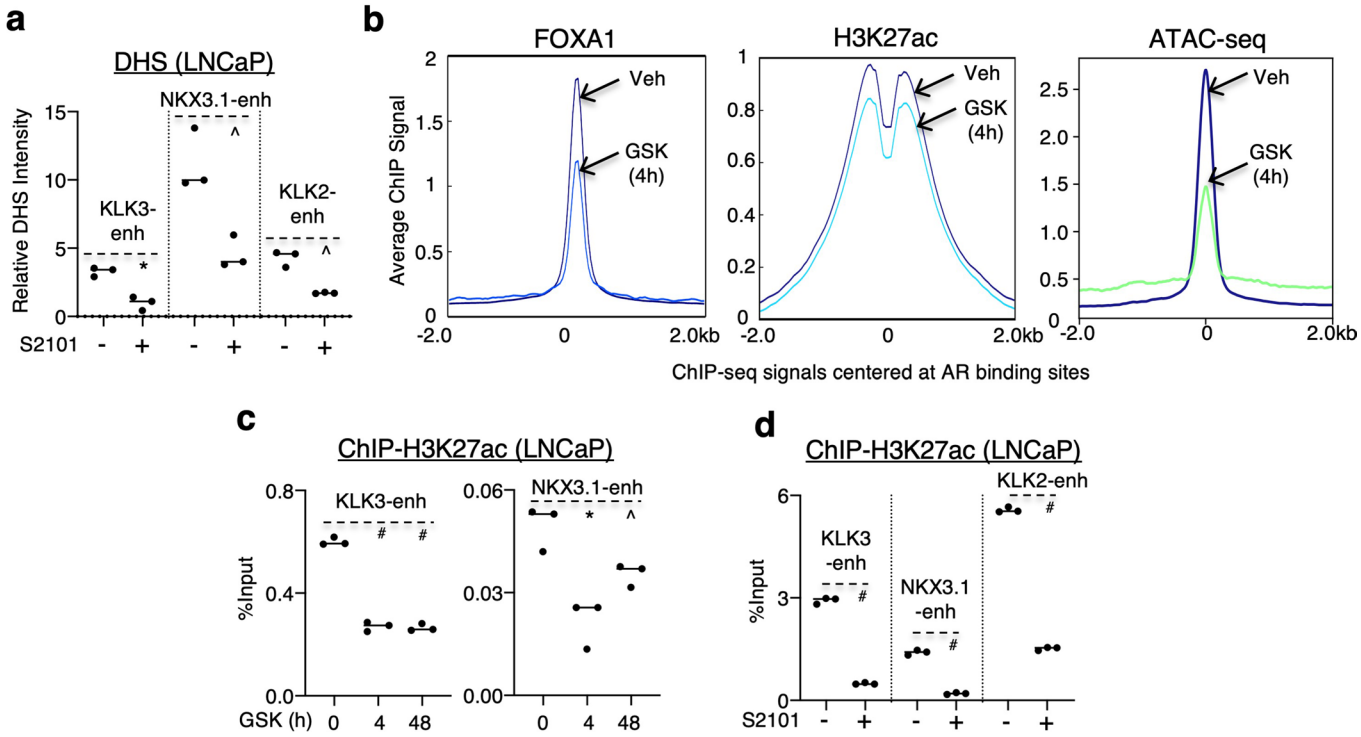

Extended Data Fig. 2 | LSD1 inhibition represses chromatin openning at FOXA1/AR mediated enhancers. a, qPCR for DHS (DNA hypersensitivity) levels at indicated enhancer sites in LNCaP cells treated with S2101 for 4 h. **b**, H3K27ac ChIP-seq was performed in LNCaP cells treated with vehicle or GSK2879552 (50 μM, 4 h). The mean values of peak intensities for FOXA1 ChIP-seq (Veh vs GSK-4h: $P = 0.03$), H3K27ac ChIP-seq (Veh vs GSK-4h: $P = 3.9 \times 10^{-12}$), and ATAC-seq at AR-binding sites (Veh vs GSK-4 h: $P = 1.4 \times 10^{-15}$) were shown. **c**, ChIP-qPCR for H3K27ac at indicated sites in LNCaP cells treated with vehicle or GSK2879552 (50 μM, 4 h). **d**, ChIP-qPCR for H3K27ac at indicated sites in CWR22-RV1 cells treated with vehicle or S2101 (50 μM, 4 h). Note: Experiments described in this figure were all done under hormone-depleted conditions.

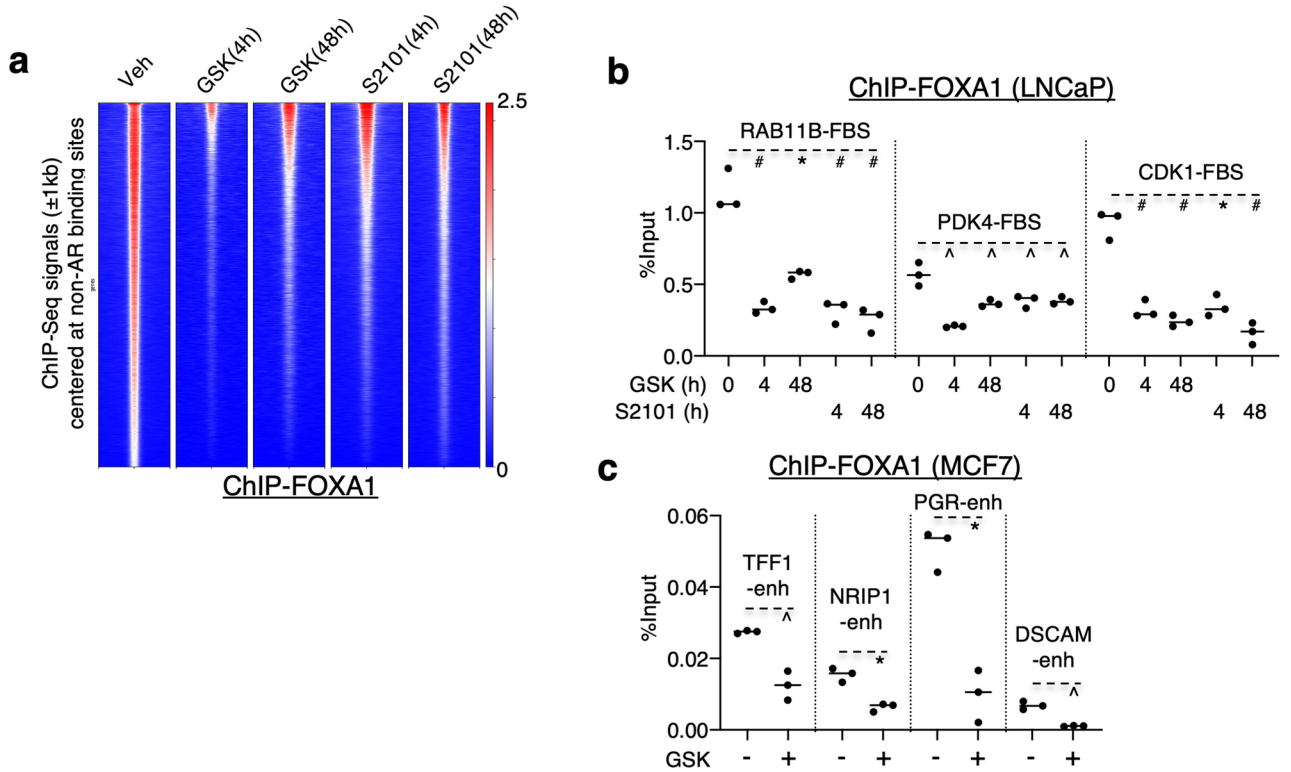

Extended Data Fig. 3 | LSD1 promotes FOXA1 binding at AR-independent regulatory sites. a, The heatmap view for FOXA1 ChIP-seq peaks at non-AR binding sites in LNCaP cells. **b**, ChIP-qPCR for FOXA1 binding at indicated non-AR binding sites (FBS: FOXA1-solo Binding Sites) in LNCaP cells treated with GSK2879552 or S2101 (50 μM, 0-48 h). c, ChIP-qPCR for FOXA1 binding at indicated ER-regulated enhancers in MCF-7 cells treated with GSK2879552 (50 μM, 4 h).

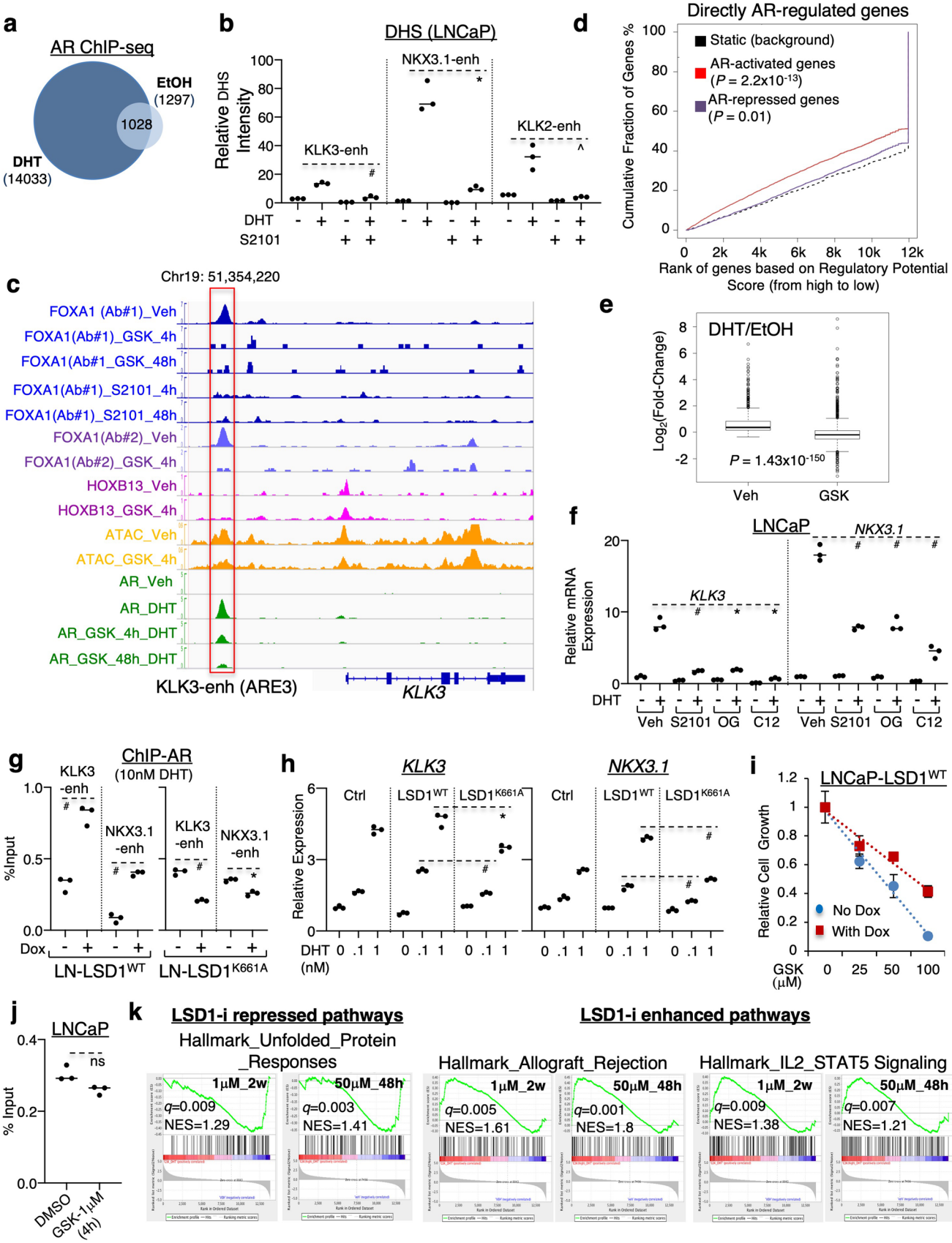

Extended Data Fig. 4 | See next page for caption.

Extended Data Fig. 4 | LSD1 enhances AR chromatin binding and activity. a, AR ChIP-seq analyses were performed in LNCaP cells treated with vehicle only, DHT (10 nM, 4 h), DHT (4 h) with pretreatment of GSK2879552 (50 μM, 0.5 h), or DHT (4 h) with pretreatment of GSK2879552 (50 μM, 48 h). Overlap of AR binding sites in vehicle and DHT treated cells was shown. **b**, qPCR for DHT-induced DHS (DNase HyperSensitivity) intensity at AR regulated enhancers in LNCaP cells pretreated with S2101 (50 μM, 0.5 h) and then treated with/without DHT (10 nM, 4 h). **c**, FOXA1, HOXB13, and AR ChIP-seq peaks as well as ATAC-seq peaks at *KLK3* locus. **d**, Identification of the subset of directly AR-regulated genes by BETA (Binding and Expression Target Analysis) using AR ChIP-seq (DHT treated for 4 h) and RNA-seq in LNCaP cells (vehicle versus DHT treated for 24 h). **e**, RNA-seq analyses in LNCaP cells treated with/without DHT (10 nM, 24 h) and with/without pretreatment of GSK2879552 (50 μM, 24 h) were performed and DHT-induced fold-change of the expression for the identified directly AR-regulated genes was plotted [center: median; box: 25th to 75th interquartile range (IQR); whiskers: 1.5x IQR; outliers: individual data points]. **f**, RT-qPCR for *PSA/NKX3.1* expression in LNCaP cells pretreated with LSD1 inhibitors for 4 h (S2101/OG-L002 at 50 μM and C12 at 5 μM) and then treated with/without DHT (10 nM, 24 h). **g**, ChIP-qPCR for AR binding in LNCaP stable cells expressing doxycycline-inducible LSD1-WT (LN-LSD1^{WT}) or LSD1-K661A (LN-LSD1^{K661A}). **h**, RT-qPCR for *KLK3* and *NKX3.1* mRNA expression in LNCaP cells stably overexpressing LSD1-WT or LSD1-K661A mutant treated with/without DHT (0-1 nM, 24 h). **i**, LN-LSD1^{WT} cells treated with different doses of GSK2879552 (6 days) and with/without doxycycline were subjected to the measurement of cell density (mean±SD). **j**, ChIP-qPCR for FOXA1 binding at *KLK3* enhancer in LNCaP cells treated with GSK2879552 (1 μM, 4 h). **k**, GSEA showing top-ranked pathways that were repressed or enhanced by GSK2879552 (1 μM for 2 weeks versus 50 μM for 48 h). Note: Experiments described in this figure were all done under hormone-depleted conditions.

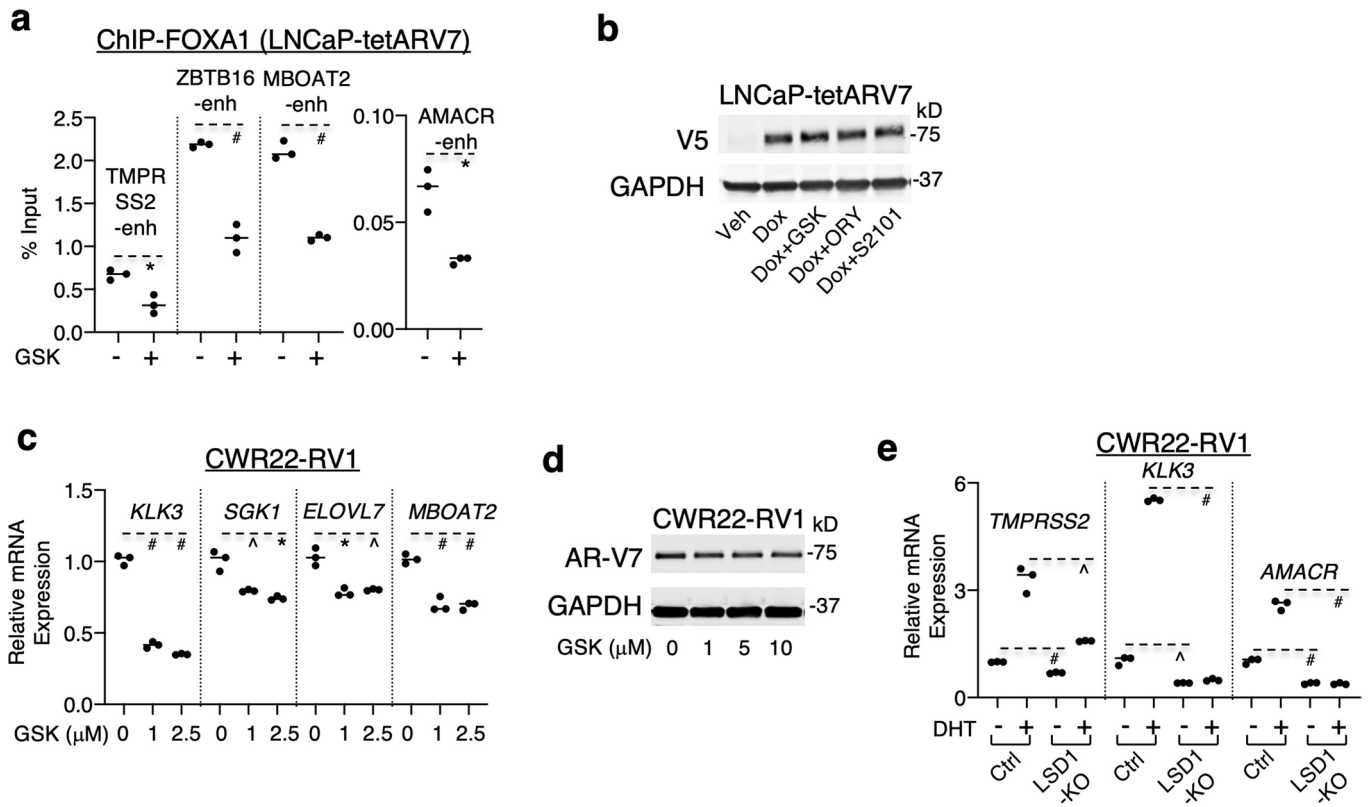

Extended Data Fig. 5 | LSD1 enhances AR-V7 chromatin binding and activity. a, ChIP-qPCR for FOXA1 binding at AR-regulated enhancers in LNCaP stable cells expressing doxycycline-inducible ARV7 (LNCaP-tetARV7) treated with/without GSK2879552 (50 μM, 4 h). **b**, Immunoblotting for V5 (AR-V7) in LNCaP-tetARV7 cells treated with vehicle, doxycycline only, doxycycline plus GSK2879552 (10 μM), doxycycline plus S2101 (10 μM), or doxycycline plus ORY-1001 (2.5 μM) for 48 h. **c**, RT-qPCR for the expression of AR-V7-regulated genes in CWR22-RV1 cells treated with GSK2879552 (0-2.5 μM for 48 h). **d**, Immunoblotting for AR-V7 in CWR22-RV1 cells treated with GSK2879552 (0-10 μM, 48 h). **e**, RT-qPCR for AR-FL/V7-regulated genes in the LSD1-KO line versus the control line with/without 10 nM DHT treatment. Note: Experiments described in this figure were all done under hormone-depleted conditions.

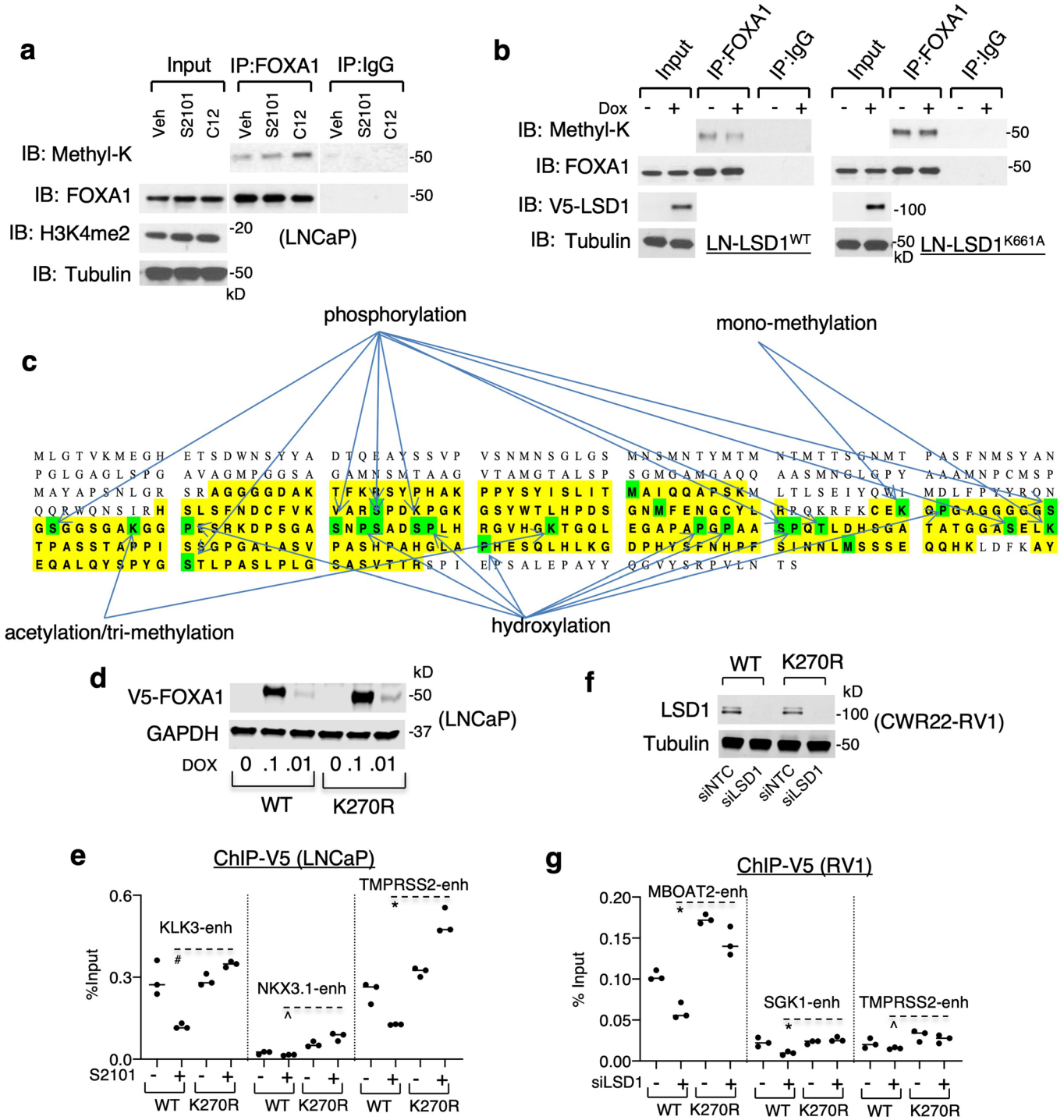

Extended Data Fig. 6 | Identification of methylated lysine 270 in FOXA1 as an LSD1 substrate. a, FOXA1 immunoprecipitation was performed in LNCaP cells treated with different LSD1 inhibitors (S2101 at 50 μM and C12 at 5 μM), followed by immunoblotting for methyllysine (images cropped from the same blot). **b**, FOXA1 immunoprecipitation was performed in LN-LSD1^{WT} or LN-LSD1^{K661A} cells, followed by immunoblotting for methyllysine. **c**, Mass-spectrometry analysis on immunoprecipitated V5-FOXA1 in LNCaP cells stably overexpressing V5-tagged FOXA1. Covered residues are in yellow. Residues with detected post-translational modifications are indicated in green. **d**, LNCaP stable cells expressing doxycycline-inducible V5-tagged FOXA1-WT (LNCaP-tetFOXA1^{WT}) or FOXA1-K270R (LNCaP-tetFOXA1^{K270R}) were generated. V5-FOXA1 expression induced by doxycycline treatment (0-0.1 μg/ml) was confirmed by immunoblotting. **e**, ChIP-qPCR for FOXA1-WT or K270R binding (anti-V5) at AR-regulated enhancers in these stable cells (doxycycline supplemented) treated with S2101 (50 μM, 24 h). **f**, **g**, CWR22-RV1 cells stably expressing doxycycline-inducible FOXA1-WT (CWR22RV1-tetFOXA1^{WT}) or K270R mutant (CWR22RV1-tetFOXA1^{K270R}) were established. Immunoblotting for LSD1 in those stable cells (doxycycline supplemented) transfected with siRNA against LSD1 (siLSD1) or non-target control (siNTC) (**f**) and ChIP-qPCR for V5-FOXA1 binding (**g**) were performed. Note: Experiments described in this figure were all done under hormone-depleted conditions.

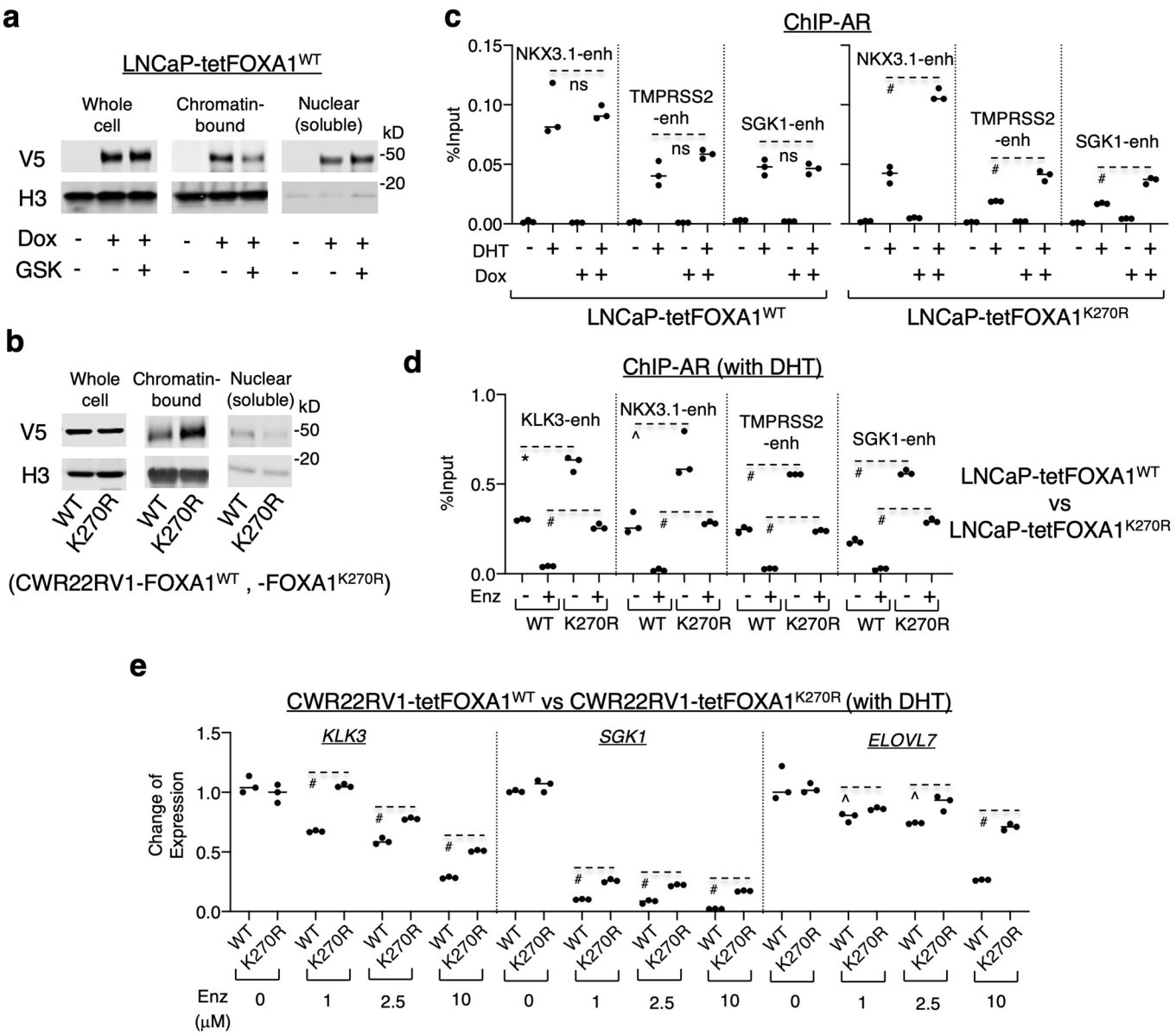

Extended Data Fig. 7 | K270R mutation of FOXA1 enhances the chromatin binding of FOXA1 and subsequently stabilizes AR recruitment. **a**, LNCaP-tetFOXA1^{WT} cells treated with GSK2879552 (50 μM) were fractionated into the soluble nuclear fraction and the insoluble chromatin-bound fraction, followed by immunoblotting for V5 and histone 3 (H3). **b**, CWR22RV1-tetFOXA1^{WT} or CWR22RV1-tetFOXA1^{K270R} cells were fractionated into the soluble nuclear fraction and the insoluble chromatin-bound fraction, followed by immunoblotting for V5 and H3. **c**, LNCaP-tetFOXA1^{WT} or LNCaP-tetFOXA1^{K270R} cells were treated with/without doxycycline for 48 h, and DHT or vehicle for 4 h. ChIP-qPCR for AR binding at AR-regulated enhancers was shown. **d**, ChIP-qPCR for AR binding in LNCaP-tetFOXA1^{WT} or LNCaP-tetFOXA1^{K270R} cells treated with DHT (10 nM) versus DHT plus enzalutamide (10 μM). **e**, RT-qPCR for androgen-induced gene expression in response to enzalutamide treatment in CWR22RV1-tetFOXA1^{WT} or CWR22RV1-tetFOXA1^{K270R} cells (in the presence of 10 nM DHT). Note: Experiments described in this figure were all done under hormone-depleted conditions.

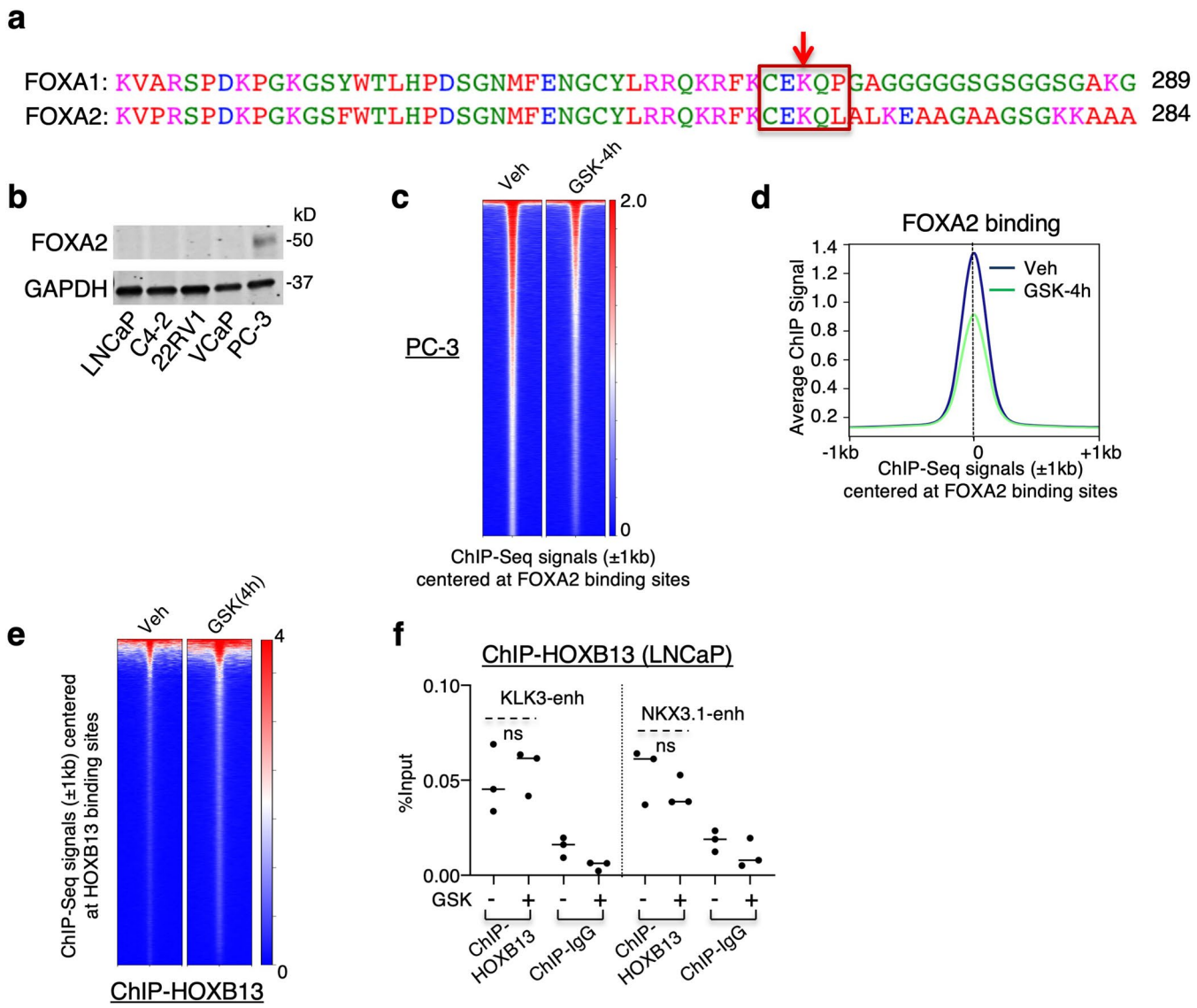

Extended Data Fig. 8 | LSD1 inhibition impairs FOXA2 binding in PC-3 cells. a, The amino acid sequences at the wing2 region of FOXA1 and FOXA2 were aligned. The red arrow indicates the K270 of FOXA1 and K265 of FOXA2. **b**, Immunoblotting for FOXA2 in the indicated PCa cell lines. **c**, **d**, FOXA2 ChIP-seq was performed in PC-3 cells treated with vehicle or GSK2879552 (50 μM, 4 h). (c) Heatmap view for FOXA2 ChIP-seq peak intensity and (d) the mean of FOXA2 ChIP-seq signals at FOXA2 binding sites (Veh vs GSK-4 h: $P = 1.6 \times 10^{-6}$) were shown. **e**, HOXB13 ChIP-seq was performed in LNCaP cells treated with vehicle or GSK2879552 (50 μM, 4 h). The heatmap view for HOXB13 ChIP-seq peak intensity was shown. **f**, ChIP-qPCR for HOXB13 binding at indicated enhancer sites in LNCaP cells treated with/without GSK2879552 (50 μM, 4 h). Note: Experiments described in this figure were all done under hormone-depleted conditions.

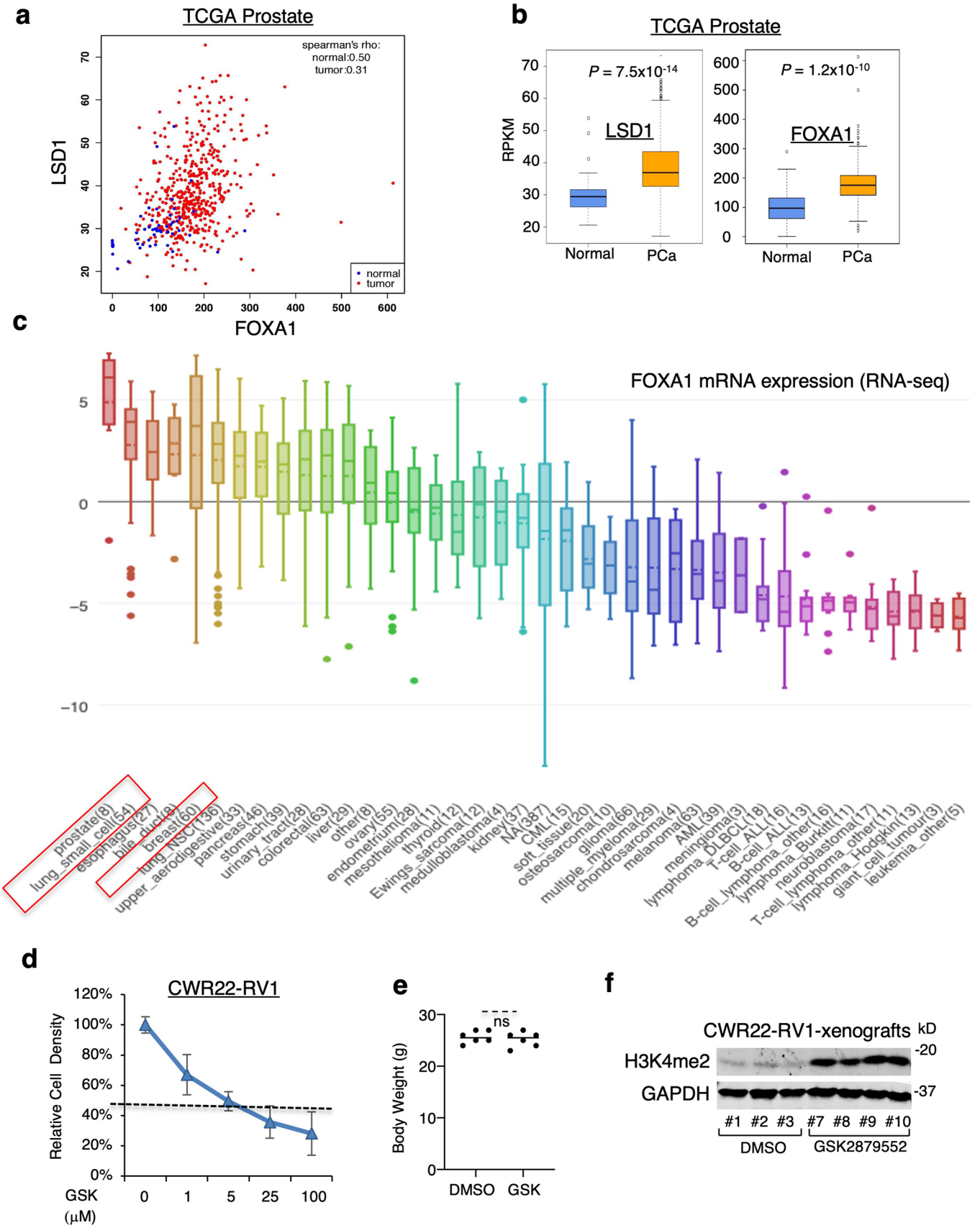

Extended Data Fig. 9 | See next page for caption.

Extended Data Fig. 9 | LSD1 inhibition suppresses tumor growth in the CWR22-RV1 CRPC model. a, The correlation between LSD1 and FOXA1 mRNA expression levels in TCGA PCa cohort. **b**, LSD1 and FOXA1 expressions in normal prostate versus PCa tumors using TCGA PCa dataset (center: median; box: 25th to 75th IQR; whiskers: 1.5x IQR; outliers: individual data points). **c**, FOXA1 mRNA expression levels in cell lines derived from different diseases using data from cancer cell line encyclopedia, CCLE (center: median; box: 25th to 75th IQR; whiskers: 1.5x IQR; outliers: individual data points). **d**, CWR22-RV1 cells (under hormone depleted condition) were treated with different doses of GSK2879552, and cell density was measured after 2 days of treatments (mean±SD). **e**, Castrated SCID male mice bearing CWR22-RV1 xenograft tumors received DMSO or GSK2879552 treatment and the body weight was measured at the endpoint. **f**, Immunoblotting for H3K4me2 in the vehicle versus GSK2879552 treated group.

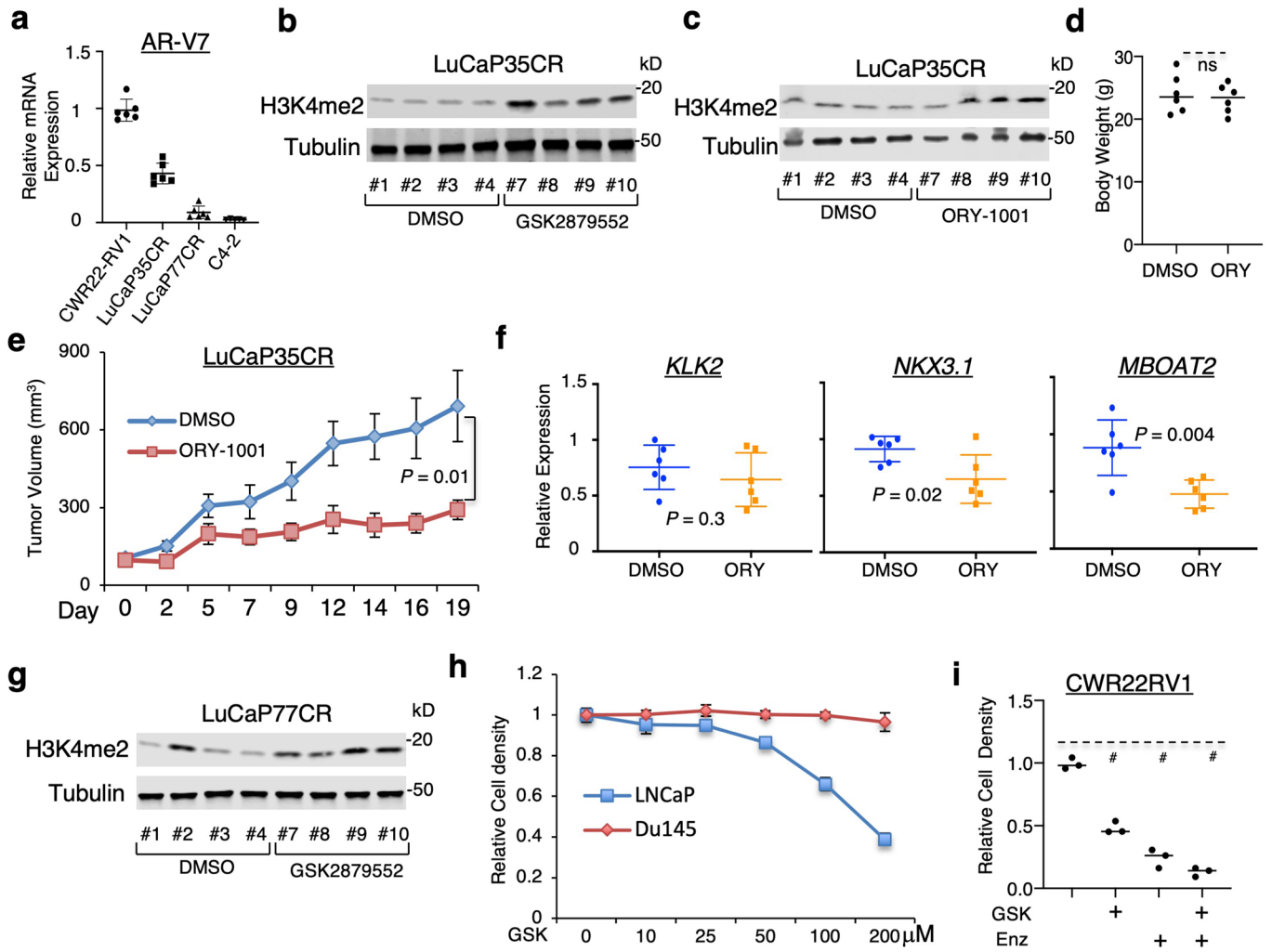

Extended Data Fig. 10 | LSD1 inhibition suppresses tumor growth of FOXA1-positive CRPC patient-derived xenograft models. a, The mRNA expression of AR-V7 was examined in tumor samples from vehicle-treated xenograft tumors in comparison with C4-2 (AR-V7 negative) derived xenograft tumors. **b**, **c**, LuCaP35CR tumors were established in castrated male SCID mice and treated with LSD1 inhibitors. Immunoblotting for H3K4me2 in LuCaP35CR treated with vehicle versus GSK2879552 (**b**) or vehicle versus ORY-1001 (**c**). **d**, Bodyweight for mice bearing LuCaP35CR treated with vehicle versus ORY-1001. **e**, **f**, Castrated SCID male mice bearing LuCaP35CR xenograft tumors received daily DMSO or ORY-1001 (0.06 mg/kg) via intraperitoneal injection (n = 7 independent tumors). (**e**) The tumor volume was measured at the indicated time. (**f**) After the mice were sacrificed, tumor samples were subjected to RT-PCR analysis for indicated AR-FL/V7 regulated genes. **g**, LuCaP77CR tumors were established in castrated male SCID mice and treated with LSD1 inhibitors. Immunoblotting for H3K4me2 in LuCaP77CR tumors treated with vehicle versus GSK2879552. **h**, LNCaP and DU145 cell lines were treated with 0-200 μM GSK2879552 for 4 days and the cell density was measured (mean±SD). **i**, CWR22-RV1 cells (under hormone depleted condition) were treated with DMSO, GSK2879552 (5 μM), enzalutamide (10 μM), or combination of GSK2879552 and enzalutamide for 2 days, and then cell density was measured.

nature research

Corresponding author(s): Changmeng Cai

Last updated by author(s): 2020-7-20

Reporting Summary

Nature Research wishes to improve the reproducibility of the work that we publish. This form provides structure for consistency and transparency in reporting. For further information on Nature Research policies, see our Editorial Policies and the Editorial Policy Checklist.

Statistics

For all statistical analyses, confirm that the following items are present in the figure legend, table legend, main text, or Methods section.

n/a	Confirmed
☐	☒ The exact sample size (*n*) for each experimental group/condition, given as a discrete number and unit of measurement
☐	☒ A statement on whether measurements were taken from distinct samples or whether the same sample was measured repeatedly
☐	☒ The statistical test(s) used AND whether they are one- or two-sided *Only common tests should be described solely by name; describe more complex techniques in the Methods section.*
☐	☒ A description of all covariates tested
☒	☐ A description of any assumptions or corrections, such as tests of normality and adjustment for multiple comparisons
☐	☒ A full description of the statistical parameters including central tendency (e.g. means) or other basic estimates (e.g. regression coefficient) AND variation (e.g. standard deviation) or associated estimates of uncertainty (e.g. confidence intervals)
☐	☒ For null hypothesis testing, the test statistic (e.g. *F*, *t*, *r*) with confidence intervals, effect sizes, degrees of freedom and *P* value noted *Give P values as exact values whenever suitable.*
☒	☐ For Bayesian analysis, information on the choice of priors and Markov chain Monte Carlo settings
☒	☐ For hierarchical and complex designs, identification of the appropriate level for tests and full reporting of outcomes
☒	☐ Estimates of effect sizes (e.g. Cohen's *d*, Pearson's *r*), indicating how they were calculated

Our web collection on statistics for biologists contains articles on many of the points above.

Software and code

Policy information about availability of computer code

Data collection	no softwares were used for data collection
Data analysis	R (version 3.4.0) was used for ChIP-seq and RNA-seq data analysis and visulaization; R package ChIPpeakAnno (version 3.10.1) was used for analyzing peak intervals; deepTools (version 2.4.1) was used to extract and visualize signal from bigwig files.bwa (version 0.7.2) was used for ChIP-seq data data mapping. samtools(v0.1.18) was used to convert sam to bam files. MACS2(v2.1.2) was used to call peak on the bam files and generate normalized bedGraph files. bedGraph files were converted to bigwig files using the ucsctool kit(315). STAR (v0.7.2) was used to map RNA-seq reads. R (version 3.4.0) was used for ChIP-seq and RNA-seq data analysis and visulaization; R package ChIPpeakAnno (version 3.10.1) was used for analyzing peak intervals; deepTools (version 2.4.1) was used to extract and visualize signal from bigwig files.

For manuscripts utilizing custom algorithms or software that are central to the research but not yet described in published literature, software must be made available to editors and reviewers. We strongly encourage code deposition in a community repository (e.g. GitHub). See the Nature Research guidelines for submitting code & software for further information.

Data

Policy information about availability of data

All manuscripts must include a data availability statement. This statement should provide the following information, where applicable:

- Accession codes, unique identifiers, or web links for publicly available datasets
- A list of figures that have associated raw data
- A description of any restrictions on data availability

Public DNase-seq and H3K4me2 ChIP-seq data were downloaded from GEO: GSM822388 and GSM503903. All in-house generated data are deposited on GEO: GSE114268.

Field-specific reporting

Please select the one below that is the best fit for your research. If you are not sure, read the appropriate sections before making your selection.

☒ Life sciences ☐ Behavioural & social sciences ☐ Ecological, evolutionary & environmental sciences

For a reference copy of the document with all sections, see nature.com/documents/nr-reporting-summary-flat.pdf

Life sciences study design

All studies must disclose on these points even when the disclosure is negative.

Sample size	Sample size was determined according to experimental design. No sample size calculation was necessary or performed. All biological specimens available were used and included in the analysis.
Data exclusions	No data excluded
Replication	Experiments were generally done in biological replicates and the replicating experiments produced similar results. Individual ChIP-seq was performed in technical duplicates and was merged for analysis.
Randomization	Samples were randomly allocated
Blinding	The experiments were performed blinded

Reporting for specific materials, systems and methods

We require information from authors about some types of materials, experimental systems and methods used in many studies. Here, indicate whether each material, system or method listed is relevant to your study. If you are not sure if a list item applies to your research, read the appropriate section before selecting a response.

Materials & experimental systems

n/a	Involved in the study
☐	☒ Antibodies
☐	☒ Eukaryotic cell lines
☒	☐ Palaeontology and archaeology
☐	☒ Animals and other organisms
☒	☐ Human research participants
☒	☐ Clinical data
☒	☐ Dual use research of concern

Methods

n/a	Involved in the study
☐	☒ ChIP-seq
☒	☐ Flow cytometry
☒	☐ MRI-based neuroimaging

Antibodies

Antibodies used	For ChIP experiments, 4ug of antibodies were used per one 15cm dish of cells. anti-FOXA1 antibody #1 (Abcam, ab23738, WB:1:2000, Lot GR3276275-1), anti-FOXA1 antibody #2 (Abcam, ab5089, Lot GR122110-6), anti-FOXA2 antibody (Millipore, 17-10258, WB:1:1000, Lot 3273958),anti-HOXB13 antibody (Cell Signaling, 90944, Lot 1), anti-H3K4me2 antibody (MIllipore, 07-030, WB:1:1000, Lot 3172453), anti-H3K27ac antibody (Abcam, ab4729, Lot GR3251519-2), anti-AR antibody (Santa Cruz, sc-815, Lot N/A), anti-V5 (Thermo Fisher, R960-25, WB:1:1000, Lot 1965106), anti-AR-V7 (Precision Antibody, AG10008, WB:1:1000, Lot 15FEB2017), anti-p300 (Abcam, ab10485, Lot GR3233406-1), anti-AR (Millipore, 06-680 WB:1:1000, Lot N/A), anti-IgG (Millipore, 12-370, Lot 3281600), anti-H3 (Abcam, ab1791, WB:1:5000, Lot GR65699-2), anti-Methyl-lysine (Abcam, ab23366, WB:1:200, Lot 20190610VD), anti-K270me (Abcam, customized, WB:1:200), anti-LSD1 (Abcam, ab17721, WB: 1:1000, GR3277379-1), anti-β-Tublin (Abcam, Ab6046, WB:1:5000, Lot GR257705-1), anti-GAPDH (Abcam, Ab8245, WB:1:5000, Lot GR3235553-2), and anti-PSA (meridianlifescience,K92110R, WB:1:1000, Lot 2009600).
Validation	FOXA1 antibodies used for ChIP-seq have been validated in publications:PMID: 25482560,PMID: 30840881. FOXA2 antibody is validated by vendor as ChIPAb+™. HOXB13 antibody is validated in PMID: 32012197 for ChIP. H3K4me2,H3K27ac, anti-V5, AR (Santa Cruz) antibodies are validated by vendor for WB and ChIP-seq. Anti-AR-V7,p300, AR (Millipore), IgG antibodies are validated by vendor for WB and ChIP. Anti-H3, LSD1, β-Tublin, GAPDH, PSA, Methyl-lysine, K270me antibodies are validated by vendor for WB.

Eukaryotic cell lines

Policy information about cell lines

Cell line source(s)	LNCaP, DU145, PC-3, CWR22-RV1,and HEK293K cells were purchased from ATCC; MCF-7 cells were kindly gifted from Dr. X. Yuan at Beth Israel Deaconess Medical Center (originally purchased from ATCC)

Authentication	Authenticated using short tandem repeat (STR) profiling
Mycoplasma contamination	Mycoplasma contamination was tested using MycoAlert kit (Lonza)and no contamination was detected
Commonly misidentified lines (See ICLAC register)	No commonly misidentified cell lines were used

Animals and other organisms

Policy information about studies involving animals; ARRIVE guidelines recommended for reporting animal research

Laboratory animals	Mouse , ICR SCID, male, 6 weeks
Wild animals	N/A
Field-collected samples	N/A
Ethics oversight	University of Massachusetts Boston

Note that full information on the approval of the study protocol must also be provided in the manuscript.

ChIP-seq

Data deposition

☒ Confirm that both raw and final processed data have been deposited in a public database such as GEO.

☒ Confirm that you have deposited or provided access to graph files (e.g. BED files) for the called peaks.

Data access links *May remain private before publication.*	https://www.ncbi.nlm.nih.gov/geo/query/acc.cgi?acc=GSE149007
Files in database submission	GSM3138620_LN_DHT_GSK4H_ARC19_merged_peaks.narrowPeak.gz GSM3138620_LN_DHT_GSK4H_ARC19_merged_treat_pileup.bdg.bw GSM3138622_LN_ARC19_merged_peaks.narrowPeak.gz GSM3138622_LN_ARC19_merged_treat_pileup.bdg.bw GSM3138624_LN_DHT_GSK2D_ARC19_merged_peaks.narrowPeak.gz GSM3138624_LN_DHT_GSK2D_ARC19_merged_treat_pileup.bdg.bw GSM3138626_LN_DHT_ARC19_merged_peaks.narrowPeak.gz GSM3138626_LN_DHT_ARC19_merged_treat_pileup.bdg.bw Galaxy1438-[LN_DHT_GSK4H_ARC19_CGCTCATT-ATAGAGGC_L002_R1_001.fastq].fastq.gz Galaxy1439-[LN_DHT_GSK4H_ARC19_CGCTCATT-ATAGAGGC_L001_R1_001.fastq].fastq.gz Galaxy1446-[LN_ARC19_TCCGGAGA-ATAGAGGC_L001_R1_001.fastq].fastq.gz Galaxy1447-[LN_ARC19_TCCGGAGA-ATAGAGGC_L002_R1_001.fastq].fastq.gz Galaxy1450-[LN_DHT_GSK2D_ARC19_GAGATTCC-TATAGCCT_L002_R1_001.fastq].fastq.gz Galaxy1451-[LN_DHT_GSK2D_ARC19_GAGATTCC-TATAGCCT_L001_R1_001.fastq].fastq.gz Galaxy1452-[LN_DHT_ARC19_CGCTCATT-TATAGCCT_L001_R1_001.fastq].fastq.gz Galaxy1453-[LN_DHT_ARC19_CGCTCATT-TATAGCCT_L002_R1_001.fastq].fastq.gz GSM3138628_LN_GSK48h_FOXA1.bw GSM3138628_LN_GSK48h_FOXA1_merged_peaks.narrowPeak.gz GSM3138630_LN_GSK4h_FOXA1.bw GSM3138630_LN_GSK4h_FOXA1_merged_peaks.narrowPeak.gz GSM3138632_LN_S210148h_FOXA1.bw GSM3138632_LN_S210148h_FOXA1_merged_peaks.narrowPeak.gz GSM3138634_LN_S21014h_FOXA1.bw GSM3138634_LN_S21014h_FOXA1_merged_peaks.narrowPeak.gz GSM3138636_LN_Veh_FOXA1.bw GSM3138636_LN_Veh_FOXA1_merged_peaks.narrowPeak.gz LN_GSK_48H_FOXA1_TCCGCGAA-CCTATCCT_L001_R1_001.fastq.gz LN_GSK_48H_FOXA1_TCCGCGAA-CCTATCCT_L002_R1_001.fastq.gz LN_GSK_4H_FOXA1_CGGCTATG-CCTATCCT_L001_R1_001.fastq.gz LN_GSK_4H_FOXA1_CGGCTATG-CCTATCCT_L002_R1_001.fastq.gz LN_S2101_48H_FOXA1_TAATGCGC-CCTATCCT_L001_R1_001.fastq.gz LN_S2101_48H_FOXA1_TAATGCGC-CCTATCCT_L002_R1_001.fastq.gz LN_S2101_4H_FOXA1_CTGAAGCT-CCTATCCT_L001_R1_001.fastq.gz LN_S2101_4H_FOXA1_CTGAAGCT-CCTATCCT_L002_R1_001.fastq.gz LN_VEH_FOXA1_GAATTCGT-CCTATCCT_L001_R1_001.fastq.gz LN_VEH_FOXA1_GAATTCGT-CCTATCCT_L002_R1_001.fastq.gz GSM3138638_LN_GSK2D_K27AC_peaks.narrowPeak.gz GSM3138638_LN_GSK2D_K27AC_treat_pileup.bdg.bw GSM3138640_LN_GSK4H_K27AC_peaks.narrowPeak.gz GSM3138640_LN_GSK4H_K27AC_treat_pileup.bdg.bw GSM3138642_LN_K27AC_peaks.narrowPeak.gz

GSM3138642_LN_K27AC_treat_pileup.bdg.bw
LN_GSK2D_K27AC_TCCGGAGA-TATAGCCT_L001_R1_001.fastq.gz
LN_GSK2D_K27AC_TCCGGAGA-TATAGCCT_L002_R1_001.fastq.gz
LN_GSK4H_K27AC_ATTACTCG-ATAGAGGC_L001_R1_001.fastq.gz
LN_GSK4H_K27AC_ATTACTCG-ATAGAGGC_L002_R1_001.fastq.gz
LN_K27AC_ATTACTCG-TATAGCCT_L001_R1_001.fastq.gz
LN_K27AC_ATTACTCG-TATAGCCT_L002_R1_001.fastq.gz
GSM3769148_LN_H3K4me2_ctrl_TCCGGAGA_peaks.narrowPeak.gz
GSM3769148_LN_H3K4me2_ctrl_TCCGGAGA_treat_pileup.bdg.bw
GSM3769150_LN_H3K4me2_GSK4_TCCGGAGA_peaks.narrowPeak.gz
GSM3769150_LN_H3K4me2_GSK4_TCCGGAGA_treat_pileup.bdg.bw
GSM3769152_LN_H3K4me2_GSK24_CGCTCATT_peaks.narrowPeak.gz
GSM3769152_LN_H3K4me2_GSK24_CGCTCATT_treat_pileup.bdg.bw
LN_H3K4me2_ctrl_TCCGGAGA-CCTATCCT_L001_R1_001.fastq.gz
LN_H3K4me2_ctrl_TCCGGAGA-CCTATCCT_L002_R1_001.fastq.gz
LN_H3K4me2_GSK4_TCCGGAGA-GGCTCTGA_L001_R1_001.fastq.gz
LN_H3K4me2_GSK4_TCCGGAGA-GGCTCTGA_L002_R1_001.fastq.gz
LN_H3K4me2_GSK24_CGCTCATT-TATAGCCT_L001_R1_001.fastq.gz
LN_H3K4me2_GSK24_CGCTCATT-TATAGCCT_L002_R1_001.fastq.gz
GSE148925_LN_ATAC_GSK_S2.bw
GSE148925_LN_ATAC_GSK_S2_peaks.narrowPeak.gz
GSE148925_LN_ATAC_VEH_S1.bw
GSE148925_LN_ATAC_VEH_S1_peaks.narrowPeak.gz
LN_ATAC_GSK_S2_L001_R1_001.fastq.gz
LN_ATAC_GSK_S2_L002_R1_001.fastq.gz
LN_ATAC_VEH_S1_L001_R1_001.fastq.gz
LN_ATAC_VEH_S1_L002_R1_001.fastq.gz
GSE148982_PC3_FOXA2_GSK_S11.bw
GSE148982_PC3_FOXA2_GSK_S11_peaks.narrowPeak.gz
GSE148982_PC3_FOXA2_S10.bw
GSE148982_PC3_FOXA2_S10_peaks.narrowPeak.gz
PC3_FOXA2_GSK_S11_L001_R1_001.fastq.gz
PC3_FOXA2_GSK_S11_L002_R1_001.fastq.gz
PC3_FOXA2_S10_L001_R1_001.fastq.gz
PC3_FOXA2_S10_L002_R1_001.fastq.gz
GSE148928_LN_HOXB13_GSK_S6.bw
GSE148928_LN_HOXB13_GSK_S6_peaks.narrowPeak.gz
GSE148928_LN_HOXB13_VEH_S5.bw
GSE148928_LN_HOXB13_VEH_S5_peaks.narrowPeak.gz
LN_HOXB13_GSK_S6_L001_R1_001.fastq.gz
LN_HOXB13_GSK_S6_L002_R1_001.fastq.gz
LN_HOXB13_VEH_S5_L001_R1_001.fastq.gz
LN_HOXB13_VEH_S5_L002_R1_001.fastq.gz
GSE148926_LN_FOXA1_G_GSK_S8.bw
GSE148926_LN_FOXA1_G_GSK_S8_peaks.narrowPeak.gz
GSE148926_LN_FOXA1_G_S7.bw
GSE148926_LN_FOXA1_G_S7_peaks.narrowPeak.gz
LN_FOXA1_G_GSK_S8_L001_R1_001.fastq.gz
LN_FOXA1_G_GSK_S8_L002_R1_001.fastq.gz
LN_FOXA1_G_S7_L001_R1_001.fastq.gz
LN_FOXA1_G_S7_L002_R1_001.fastq.gz

Genome browser session
(e.g. UCSC)

N/A

Methodology

Replicates

Experiments were performed in two technical replicates and were pooled for analysis

Sequencing depth

ChIP-seq were 51 bp single-end
sample_name total_reads uniquely_mapped_reads
LN_ARC19_L001 17520657 16084755
LN_ARC19_L002 18137016 16673883
LN_DHT_ARC19_L001 13237866 12365174
LN_DHT_ARC19_L002 13798255 12893586
LN_DHT_GSK2D_ARC19_L001 17618661 16541726
LN_DHT_GSK2D_ARC19_L002 18158955 17071042
LN_DHT_GSK4H_ARC19_L001 15850426 14858659
LN_DHT_GSK4H_ARC19_L002 16525490 15495105
LN_GSK_48H_FOXA1_L1 8797380 6872214
LN_GSK_48H_FOXA1_L2 9114869 7127979
LN_GSK_4H_FOXA1_L1 9942548 7452349
LN_GSK_4H_FOXA1_L2 10355272 7763087
LN_S2101_48H_FOXA1_L1 9183665 7365792

LN_S2101_48H_FOXA1_L2 9477591 7626558
LN_S2101_4H_FOXA1_L1 10070883 8469291
LN_S2101_4H_FOXA1_L2 10434906 8795467
LN_VEH_FOXA1_L1 2677474 2617852
LN_VEH_FOXA1_L2 2784767 2723090
LN_GSK2D_K27AC_rep1 12309893 11439072
LN_GSK2D_K27AC_rep2 12723262 11837430
LN_GSK4H_K27AC_rep1 14117484 12789252
LN_GSK4H_K27AC_rep2 14516444 13172951
LN_K27AC_rep1 12062417 11003614
LN_K27AC_rep2 12416101 11344602
LN_Veh_H3K4me2_rep1 15933167 14491802
LN_Veh_H3K4me2_rep2 16183088 14724831
LN_GSK4H_H3K4me2_rep1 14510691 14215634
LN_GSK4H_H3K4me2_rep2 14731393 14432035
LN_GSK24H_H3K4me2_rep1 14596727 12542477
LN_GSK24H_H3K4me2_rep2 14895987 12804033
RV_V5FOXA1_WT_GSK_rep1 7798230 7336946
RV_V5FOXA1_WT_GSK_rep2 7911122 7445628
RV_V5FOXA1_K270R_GSK 11378183 10813102
RV_V5FOXA1_K270R_GSK 11619996 11045995
RV_AR_K270R_rep1 12606105 6558855
RV_AR_K270R_rep2 12583340 6534984
RV_AR_WT_rep1 12307894 3310480
RV_AR_WT_rep2 12299854 3298752
LN_ATAC_GSK_S2_L1 62142484 59887503
LN_ATAC_GSK_S2_L2 63472683 61163836
LN_ATAC_VEH_S1_L1 54033489 51916484
LN_ATAC_VEH_S1_L2 55316179 53150981
LN_FOXA1_GSK_S8_L1 8997775 4942227
LN_FOXA1_GSK_S8_L2 9153659 5032517
LN_FOXA1_S7_L1 13049492 12163634
LN_FOXA1_S7_L2 13288961 12379445
PC3_FOXA2_GSK_S11_L1 13168236 10640625
PC3_FOXA2_GSK_S11_L2 13375887 10810072
PC3_FOXA2_S10_L1 12259150 10135750
PC3_FOXA2_S10_L2 12471436 10313322
LN_GSK_HOXB13_S6_L1 36313273 30785964
LN_GSK_HOXB13_S6_L2 36883221 31281546
LN_Veh_HOXB13_S5_L1 6751854 6178976
LN_Veh_HOXB13_S5_L2 6855271 6273146

Antibodies

anti-FOXA1 antibody #1 (Abcam, ab23738), anti-FOXA1 antibody #2 (Abcam, ab5089), anti-FOXA2 antibody (Millipore, 17-10258),anti-HOXB13 antibody (Cell Signaling, 90944), anti-H3K4me2 antibody (MIllipore, 07-030), anti-H3K27ac antibody (Abcam, ab4729), anti-AR antibody (Santa Cruz, sc-815), anti-V5 (Thermo Fisher, R960-25)

Peak calling parameters

bwa aln: -q 5 -l 32 -k 2 -t 8
bwa samse: default parameters
samtools view defalut parameter for converting sam to bam
macs2 callpeak: --bw 250 --mfold 10 30 --extsize 100 --seed 1 --fix-bimodal --qvalue 0.05 --SPMR -B
bedClip and bedGraphToBigWig for converting bdg to bw

Data quality

fastqc was run on all samples to confirm data were of good quality
Sample_name Peak_number
LN_ARC19_merged 831
LN_DHT_ARC19_merged 11891
LN_DHT_GSK2D_ARC19_merged 5484
LN_DHT_GSK4H_ARC19_merged 7175
LN_GSK_48H_FOXA1_merged 10492
LN_GSK_4H_FOXA1_merged 6464
LN_S2101_48H_FOXA1_merged 24424
LN_S2101_4H_FOXA1_merged 33845
LN_VEH_FOXA1_merged 49919
LN_GSK2D_K27AC_merged 40556
LN_GSK4H_K27AC_merged 36811
LN_K27AC_merged 37146
LN_Veh_H3K4me2_merged 101165
LN_GSK4H_H3K4me2_merged 129776
LN_GSK24H_H3K4me2_merged 128552
RV_V5FOXA1_WT_GSK_merged 3653
RV_V5FOXA1_K270R_GSK_merged 12971
RV_AR_K270R_merged 53918
RV_AR_WT 7070
LN_ATAC_GSK 163735
LN_ATAC_VEH 194551
LN_FOXA1 (Ab#2)_GSK 28485

LN_FOXA1 (Ab#2) 149340
PC3_FOXA2_GSK 14846
PC3_FOXA2 21308
LN_GSK_HOXB13 68725
LN_Veh_HOXB13 3722

Software

bwa (version 0.7.2)
samtools (version 0.1.18)
MACS2 (version 2.1.2)
ucsctool kit (315)
R package ChIPpeakAnno (version 3.10.1)
deepTools (version 2.4.1)